MECHANICAL PROBING OF MALARIA-INFECTED ERYTHROCYTES

QIE LAN
(B.Sc., Fudan University)

A THESIS SUBMITTED

FOR THE DEGREE OF MASTER OF SCIENCE

GRADUATE PROGRAMME IN BIOENGINEERING

NATIONAL UNIVERSITY OF SINGAPORE

2005

ACKNOWLEDGEMENTS

I am greatly indebted to my supervisors, Dr Han Ming Yong, who provided me sound training in biological experimental skills and supported me right from the beginning of my thesis project, and Dr Lim Chwee Teck, who guided me with dedication all the way through this work, who offered all the laboratory facilities, experimental materials, the intelligence input, and most cherishable, all the encouragement that I needed to make this happen.

Millions of thanks to my dear coworker John Philip Mills, currently a PhD candidate at MIT. We worked together for three months on this project and shared the exhaustion & joy of working into late nights.

I would like to thank all my colleagues in the lab: Li Ang, Zhou Enhua, Lee Yew Yong Gregory, Vedula Sri Ram Krishna, Tan Phay Shing, Eunice, Xu Xiaojing, Hairul Nizam Bin Ramli. It has been a real pleasure to work with them.

Special thanks to the following people who have offered great help to this work in one way or another:

- At Department of Materials Science and Engineering, Massachusetts Institute of Technology,

  Prof. Subra Suresh, Dr. Dao Ming

- At Department of Microbiology, NUS,

  Dr Tan Shyong Wei, Kevin, Ng Geok Choo, Ramachandran, N P

TABLE OF CONTENTS

LIST OF TABLES

LIST OF FIGURES

ABBREVIATIONS

RBC	Red blood cell
Hb	Haemoglobin
MZ	Merozoite
PV	parasitophorous vacuole
PfEMP1	*Plasmodium falciparum* Erythrocyte Membrane Protein 1
CSA	chondroitin sulphate A
KAHRP	Knob-associated Histidine-rich Protein
PfEMP3	*Plasmodium falciparum* Erythrocyte Membrane Protein 3
MESA	Mature-parasite-infected Erythrocyte Surface Antigen
RESA	Ring-infected Erythrocyte Surface Antigen
FRAP	Fluorescence Recovery After Photobleaching
pN	Piconewton
AFM	Atomic Force Microscopy
MA	Micropipette Aspiration
PBS	Phosphate Buffered Saline
BSA	Bovine Serum Albumin
Hh-RBC	Healthy human RBC
Pf-U-RBC	exposed to *Plasmodium falciparum* but uninfected human RBC
Pf-R-RBC	*Plasmodium falciparum* parasitized human RBC at ring form stage

Pf-T-RBC	*Plasmodium falciparum* parasitized human RBC at trophozoite stage
Pf-S-RBC	*Plasmodium falciparum* parasitized human RBC at schizont stage
Hm-RBC	Healthy mouse RBC
Py-U-RBC	exposed to *Plasmodium yoelii* but uninfected mouse RBC
Py-R-RBC	*Plasmodium yoelii* parasitized mouse RBC at ring form stage
Py-T-RBC	*Plasmodium yoelii* parasitized mouse RBC at trophozoite stage
Py-S-RBC	*Plasmodium yoelii* parasitized mouse RBC at schizont stage
DAPI	4', 6-diamidino-2-phenylindole, dihydrochloride hydrate
FEM	Finite Element Model

SUMMARY

One of the key features of the biology and pathophysiology of the *Plasmodium* malaria is enhanced rigidification of the infected red blood cell. Some proteins released from the parasite are believed to induce alterations of the membrane skeleton and mechanical properties of the red blood cell.

Previous studies primarily used micropipette aspiration and laminar shear flow to probe cell deformability. Yet comprehensive experiments of progressive changes to nonlinear mechanical response of infected RBCs are presently unavailable.

In this work, optical tweezers was employed to obtain the first direct and continuous force-deformation responses from *in-vitro* stretching of malaria-infected RBCs from both human and rodent at various developmental stages: ring form, trophozoite and schizont stage, of *Plasmodium falciparum* within red blood cells.

Two silica micro-beads of 4.12 μm in diameter are attached diametrically across a RBC. One micro-bead is adhered to the glass surface while the other is being trapped and pulled using the optical tweezers. The whole process is recorded by a video camera and subsequently analyzed to extract the variations in cell diameters against stretch force. The parasite was also visualized using fluorescent labelling while the host red blood cell was being stretched by the optical tweezers.

By combining three-dimensional computational simulations of stretch deformation, an order of magnitude increase in shear modulus was estimated in red blood cell infected by the schizont stage parasite.

This optical tweezers approach will offer a new framework to understand the link between alteration to mechanical characteristics of parasitized cells and disease state.

Chapter 1: Introduction

1.1 Background

A healthy human red blood cell (RBC) or erythrocyte possesses mechanical properties that enable it to perform its biological function of transporting oxygen from the lungs to tissues, and carbon dioxide from respirating cells in tissues to the alveoli of lungs. With a biconcave or discocyte shape and a diameter of about 8 μm, the RBC passes through narrow capillaries with much smaller inner diameter. There, it undergoes large, reversible, nonlinear elastic deformation with strains in excess of 100%. The RBC also severely deforms through intercellular gaps of sinusoids in the spleen where stiffened and aged RBCs are removed.

The deformability of a normal RBC is facilitated by a complex cytoskeletal network which comprises spectrin molecules anchored at actin nodes, and proteins 4.1, 4.2, ankyrin and adducin [1, 2]. Interactions involving ankyrin, the RBC anion transporter band 3, protein 4.1 and sialoglycoproteins such as glycoprotein A facilitate connections between elastic membrane and cytoskeleton.

This deformability is severely hampered by malaria, which is the most widespread parasitic disease inflicting humans and which results in 2 or 3 millions of infant deaths annually. When an RBC is invaded by the *P. falciparum* parasite**,** it experiences increased propensity for adherence to linings of small blood vessels, thereby promoting parasite sequestration and obstruction to tissue perfusion [1].

Consequences of these effects of *P. falciparum* include abnormal microcirculatory responses and parasite accumulation in the microvasculature of different organs. Enhanced rigidification of RBC is a key feature of the biology and pathophysiology of malaria whose mechanisms are influenced by proteins transported from the intracellular parasite to the cell membrane and the associated alterations to the spectrin molecular network underneath the phospholipid bilayer [1-3]. Consequently, quantitative understanding of the systematic changes to deformation characteristics of parasitized RBC, that exploit latest advances in nanomechanical experimentation, would provide critical insights into possible connections among subcellular structure evolution, elastic properties of cell membrane and disease states.

Some studies have demonstrated severe stiffening of the RBC infected with *P. falciparum* by recourse to micropipette aspiration experiments [3-6]. Considerable uncertainty can arise in mechanical property extraction from micropipette aspiration experiments because of (a) feasibility to aspirate the stiffened RBC only partially into the micropipette [3], (b) geometric and mechanical artifacts induced by the stress singularity at the site of aspiration of the cell into the micropipette, (c) strong adhesion of cell membrane to the inner wall of micropipette in the later stages of culturing [3], and (d) extraction of elastic properties based on simple analysis which do not account properly for discocyte cell shape or nonlinear deformation.

In another study [7] on deformability of RBCs parasitized by *P. falciparum* and *P. vivax* to different developmental stages in a laminar shear flow system, mechanical

deformation characteristics in the advanced (schizont) stages of erythrocytic development could not be determined because of experimental difficulties. To our knowledge, no systematic studies of the progressive stiffening with the maturation of malaria parasite inside RBCs has thus far been studied in terms of direct and continuous force-displacement measurements obtained from the early ring stage to the late schizont stage. This information on stage-specific deformation characteristics is essential for systematically assessing the contributions of the malaria parasite to the mechanical deformability of the RBC. Proper interpretation of such studies will lead to better understanding of the malaria pathophysiology and new insights on how the efficacy of antimalarials can be quantitatively probed.

1.2 Objectives

The objectives of this study are:

1. To investigate the deformation characteristics of:
    a. healthy human RBCs,
    b. *Plasmodium falciparum* malaria infected human RBCs at the ring form, trophozoite and schizont developmental stages, and
    c. *Plasmodium yoelii* malaria infected rodent RBCs at the ring form, trophozoite and schizont developmental stages

    using the optical tweezers method.
2. To obtain changes in mechanical properties of each stage of both the human and rodent RBCs which will give quantitative information on the stiffening effect of the parasite infestation.

3. To conduct comparative studies of the deformation characteristics caused by *Plasmodium falciparum* and *Plasmodium yoelii* infestations. This will enable us to explore the possibility of using rodent malaria as convenient models for human malarias.

1.3 Scope

This thesis will begin with an introduction on the RBC and the *Plasmodium falciparum* malaria. A brief review will be given on previous works done to characterize the alterations on deformation properties of RBCs infected by this parasite using a variety of experimental techniques, including the optical tweezers. The present approach using optical tweezers technique will be described in the "Experimental Methods and Materials" chapter. Results of these experiments will be presented and discussed. This work will then be concluded with recommendations made for future work.

Chapter 2: Literature Review

2.1 Function and Structure of RBC

2.1.1 Human RBC

RBC is a predominant constituent in the blood. They normally occupy approximately 45% of the blood volume and account for 99.9% of the formed blood elements in human. One microliter of whole blood contains 4.5-6.3 million RBCs in adult males and 4.2-5.5 in adult females. RBCs contain the red pigment hemoglobin, which binds and transport oxygen and carbon dioxide, giving whole blood its deep red color.

(a) (b)

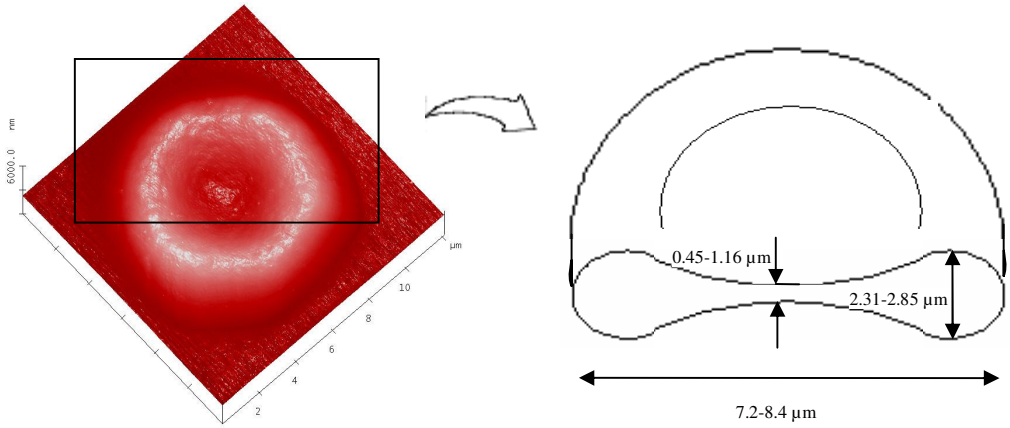

Figure 2.1 (a) AFM image showing the distinctively three-dimensional biconcave structure of a human RBC, (courtesy of Li Ang from Nano Biomechanics Lab, National University of Singapore). (b) A sectional schematic view of a mature red blood cell, showing the normal ranges of its dimensions. (Data on dimensions adapted from *Fundamentals of Anatomy & Physiology*, 6th ed.[8])

RBC is a highly specialized cell type of the human body. It has a unique biconcave disc-like shape with a thin central region and a thicker outer margin. Normal RBC has an average diameter of 7.8 µm and a maximum thickness of 2.6µm at the rim and minimum thickness of only about 0.8 µm at the center (Fig 2.1). This unusual shape has three important effects on RBC function:

1) It gives each RBC a large surface area to volume ratio. The oxygen carried by the RBC intracellular proteins must be absorbed or released quickly as the RBC passes through the capillaries of the lungs or peripheral tissues. The greater the surface area per unit volume, the faster is the exchange between the cell's interior and the surrounding plasma.
2) It enables RBCs to form stacks when traveling through relatively narrow capillaries and smooth the flow. These stacks form and dissociate repeatedly without affecting the cells involved. An entire stack can pass along a blood vessel only slightly larger than the diameter of a single RBC, whereas individual cells would bump the walls, bang together, and form logjams that could restrict or prevent blood flow.
3) It enables RBCs to bend and flex when entering small capillaries and branches. RBCs are very flexible. By changing shape, individual RBC can fold and squeeze through capillaries as narrow as 3µm, which is less than half of the diameter of RBC itself.

It takes an RBC only about 25 seconds for a single round-trip from the heart, through the peripheral tissue, and back to the heart. At this speed, an RBC gets pumped out of

the heart and forced along vessels, bouncing against the vessel walls and other RBCs, forming stacks, or squeezing through the tiny capillaries. With all this wear and tear but no repair mechanisms, a typical RBC has a relatively short life span of about 120 days, during which it travels about 700 miles. About one percent of circulating RBCs in the body are replaced each day.

2.1.2 The RBC membrane

The human erythrocyte membrane consists of 50-52% protein, 40% lipid, and 8-10% carbohydrate [9]. The structure of the red blood cell membrane is represented as a plasma membrane envelope anchored to a network of skeletal proteins through binding sites (transmembrane proteins) [10] as shown in the schematic diagram in Figure 2.2. The outer plasma membrane is essentially a lipid bilayer arranged according to the Singer-Nicolson fluid mosaic model [11] with insertion of protein components (intrinsic proteins). The intrinsic proteins include two important proteins: band 3 and glycophorin C, which are dominant in a number of molecules in the lipid layer, and all the protein molecules of channels, pumps, and glycoproteins that penetrate the lipid membrane. Most of the outside of the lipid bilayer is covered with sugar moiety of glycolipids and glycoproteins of the intrinsic proteins.

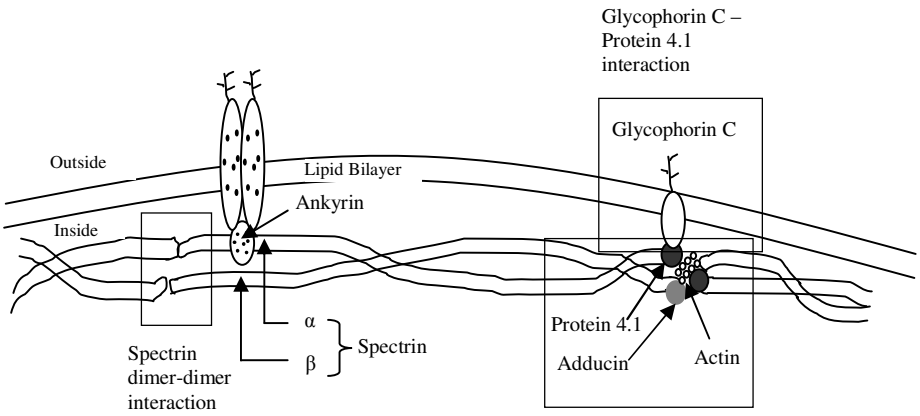

Figure 2.2 Schematic diagram of the RBC membrane organization based on current understanding of various protein associations. (Adapted from Mohandas and Chasis, 1993 [10])

The key components of the skeletal network are spectrin, actin, protein 4.1, and adducin [12-15]. Spectrin is a flexible, rodlike molecule composed of two nonidentical subunits, α spectrin and β spectrin, intertwined side-to-side to form a heterodimer. Spectrin heterodimers associated head-to-head to form $(\alpha\beta)_2$ tetrameters, which have a contour length of approximately 200 nm. It is these tetrameric species of spectrin that predominate in the membrane skeleton. At the tail ends of the spectrin tetramers are associated with actin oligomers. These RBC actin filaments are strictly organized into short, highly uniform oligomers composed of 12 monomers, approximately 35 nm in length. An irregular network is formed by six spectrin ends associating with each actin oligomer to create something like a hexagonal lattice (Figure 2.3). Occasionally, the arms of the hexagons are formed by double tetramers

or hexamers, as shown in this figure. Although individual spectrin-actin interactions are weak, the network is greatly stabilized by protein 4.1 by its direct interaction with spectrin at the junction. Adducin is another protein that stabilizes the spectrin-actin interaction.

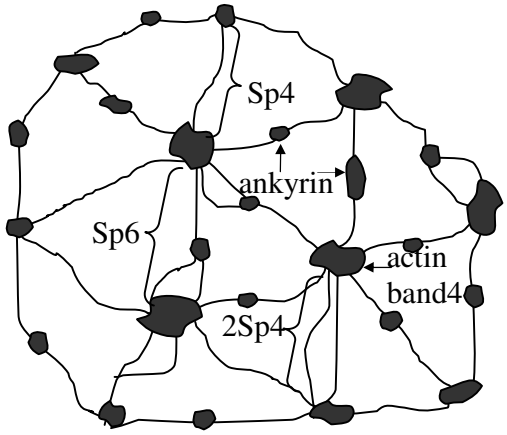

Figure 2.3 The structural elements of membrane skeleton are given in this schematic diagram showing the hexagonal lattice of junctional complexes. The arms of each polygon are formed by spectrin tetramers (Sp4) and, occasionally, double tetramers (2Sp4) or hexamers (Sp6). (Adapted from Liu *et al*., 1987 [16])

There are two most important linkages of membrane skeleton to the lipid bilayer. The primary one is ankyrin, which simultaneously interacts with spectrin in the skeleton and band 3 in the bilayer. The second linkage is achieved through interaction of the membrane intrinsic protein glycophorin C with the skeletal component protein 4.1. The lipid bilayer is therefore mechanically coupled to the membrane skeleton. Also involved in the network are some other accessory proteins such as tropomyosin, adducin and calmodulin.

2.1.3 RBC membrane deformation

The human RBC, as described before, can undergo large deformation. A model has been established to conceptualize how membrane deformation may be regulated by the skeletal network (Figure 2.4) [17]. In the nondeformed state, spectrin molecules exist in a folded conformation. Reversible deformation of the RBC membrane occurs with a change in geometric shape but at constant surface area. During reversible deformation, the skeletal network rearranges itself where certain spectrin molecules uncoil and extend, while others become more compressed and folded. The reversible deformation reaches its limit when some of the spectrin molecules increasingly stretch themselves and finally attain their maximal linear extension. Beyond this point failure will occur, leading to membrane fragmentation.

An increase in intermolecular or intramolecular associations of the skeletal proteins or an increased association of the cytoplasmic domains of membrane intrinsic proteins with the skeletal network will significantly limit the ability of spectrin molecules to rearrange and consequently, inhibit the ability of the membrane to undergo deformation. In addition, interaction of cytoplasmic hemoglobin with membrane can also affect the deformation capability of the RBC [18-21]. However, membrane lipids contribute little to the macroscopic deformations such as those induced by fluid forces in circulation [10]. The red blood cell membrane is highly deformable and tolerant against mechanical stress and various pH and salt concentrations *in vivo* and *in vitro*. The normal RBC can undergo linear extensions of

up to 250% of its original dimension, but an increase of even 3% to 4% in surface area results in cell lysis [22].

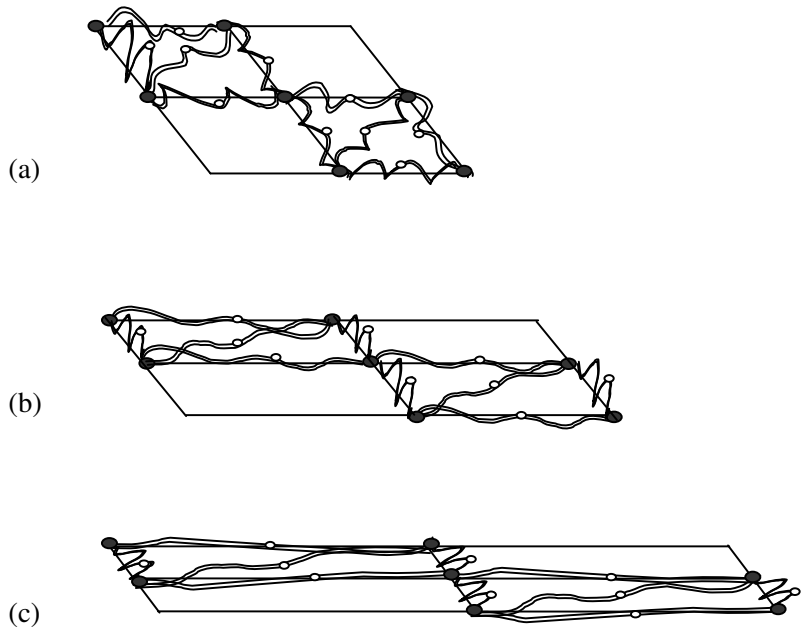

Figure 2.4 Model of reversible deformation of erythrocyte membrane. Reversible deformation occurs with a change in geometric shape but at a constant surface area. (a) The nondeformed membrane. With increased shear stress, the membrane becomes increasingly extended (b and c). Further extension of the membrane beyond that shown in (c) would result in an increase in surface area and the breaking of junction points. This is the stage at which membrane fragmentation occurs. (●, protein 4.1, actin, and spectrin association points; o, spectrin-spectrin association points; linear coils, spectrin dimer.) (Adapted from Chasis and Mohandas, 1986 [17])

2.2 Human Malaria

2.2.1 Introduction

Malaria is one of the most serious and widespread parasitic diseases on earth, it causes up to 2.7 million deaths each year, mostly children, and threatens the lives of more than one-third of the world's population. It is caused by a one-celled parasite *Plasmodium* and is typically transmitted by mosquitoes belonging to the genus *Anopheles*. Malaria thrives in the tropical areas of Asia, Africa and South and Central America. With prompt treatment, however, it is almost always curable. Chloroquine has been a highly effective medicine for preventing and treating malaria. Nonetheless, due to the ubiquity of the organism, the developing drug resistant strains, and difficulties in terms of administrative and financial matters, malaria remains to be a major killer of humans worldwide.

There are four species of *Plasmodium* that naturally infect human – *Plasmodium vivax, Plasmodium malariae, Plasmodium ovale and Plasmodium falciparum.* While all of them can result in severe morbidity, nearly all the mortality is caused by *P. falciparum,* due to two important characteristics. First, it is able to reach much higher levels of parasitaemia than other species, and second, it possesses the unique property of sequestration. Red blood cells infected with the parasites circulate freely in their early stages, whereas towards developing into more mature or late stages, infected red cells tend to adhere to endothelial cells and thus are sequestered away from the peripheral circulation and spleen filtration [1]. When parasites accumulate in large numbers in specific organ beds, damage to that organ may follow, leading to severe

disease or death. The best-studied situation results from the concentration of infected red blood cells in the brain, which can lead to cerebral malaria, coma, and death.

2.2.2 Life Cycle of the human malaria parasite

The human malaria parasite has a complex life cycle involving both a human host and an insect host. The *Anopheles* mosquitoes host *Plasmodium*'s sexual stage and once infect a human, the parasite enters its asexual stage.

When an infected female *Anopheles* bites a human, it injects saliva that contains thread-like sporozoites of the parasite into the human's bloodstream. The sporozoites are promptly transported to the liver and invade hepatocytes. There, within a week or two (depending on the *Plasmodium* species), a parasite matures, differentiates, and asexually develops into many thousands of merozoites that are then released into the bloodstream. During this time the individual does not show any clinical symptoms.

Once released into the bloodstream, the merozoites invade red blood cells immediately. This begins the asexual blood stage (see Fig 2.5) of the parasite's life cycle when the clinical symptoms occur. Within the red blood cell, the parasite feeds on hemoglobin and goes through another round of asexual reproduction. It develops into a trophozoite and finally a schizont containing many merozoites. When the schizont matures, the cell ruptures and the merozoites burst out. The newly released merozoites invade other red blood cells and the infection continues its cycle until either the host dies or the parasite is brought under control, by medicine or the body's

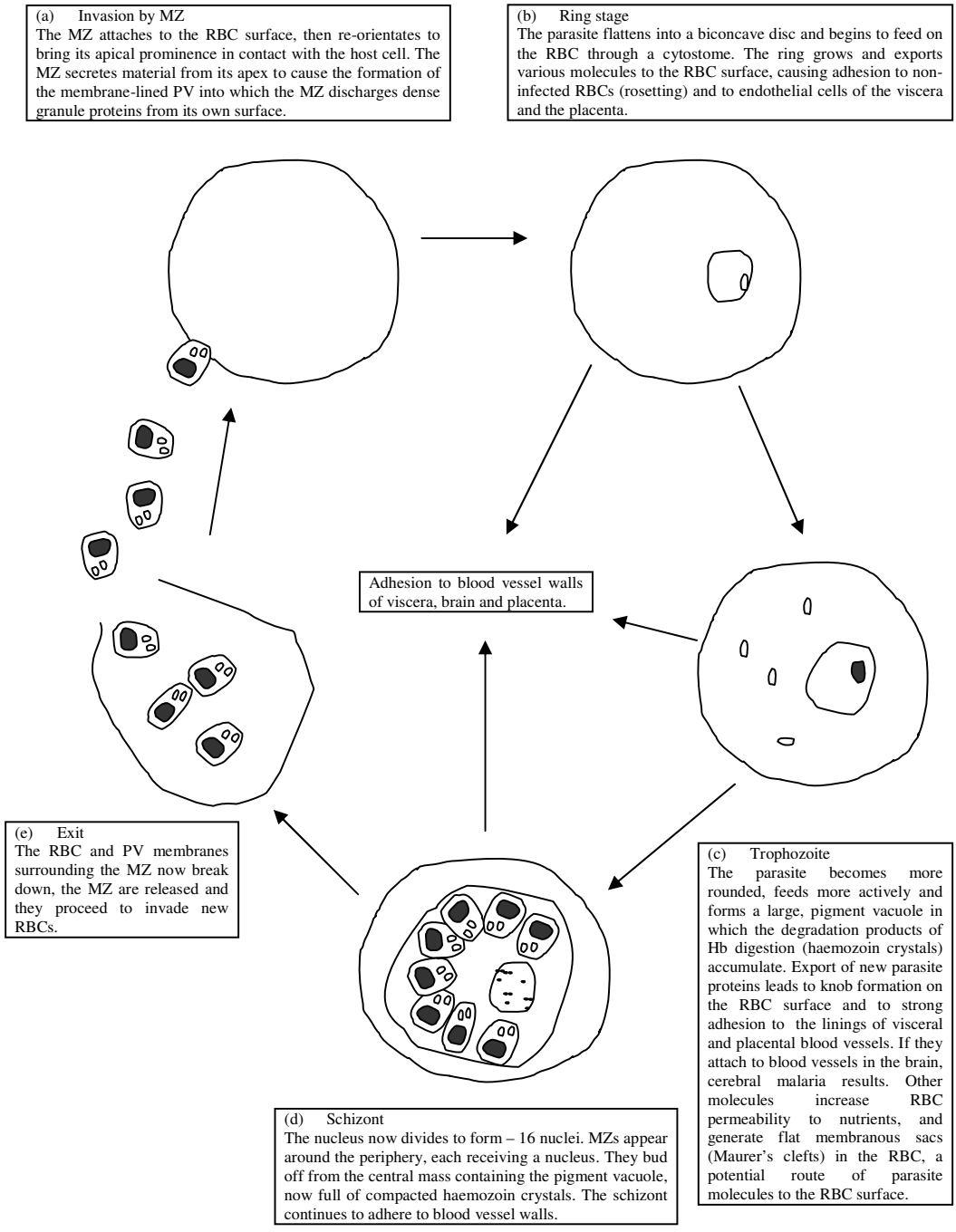

Figure 2.5 The main stages of the asexual erythrocytic cycle of *Plasmodium falciparum*. (Adapted from Bannister and Mitchell, 2003 [23]) Hb, haemoglobin; MZ, merozoite; PV, parasitophorous vacuole.

immune defenses. The exponential growth of the parasite is responsible for most of the clinical features of malaria. Because the growth within the red blood cell is roughly synchronous, erythrocyte rupture and concomitant release of the pyrogen tend to occur at the same time of day and coincide with the onset of periodic fevers. Hence the disease used to be well known as "fever and ague".

A small proportion of the merozoites undergo an alternative pathway and differentiate into male and female gametocytes. These circulate in the person's blood and may be taken up by a female *Anopheles,* where male and female gametocytes develop into gametes and fuse to form oocysts filled with infectious sporozoites. When the oocyst mature and rupture, the sporozoites are released and migrate to the mosquito's salivary gland. The cycle starts all over again with the next bite.

2.2.3 Molecular and structural changes of RBC caused by Plasmodium falciparum

Table 2.1 shows an overview of *Plasmodium falciparum* induced proteins and native proteins altered during malaria infection. Detailed description of these are given below.

Table 2.1 Protein alterations induced by *Plasmodium falciparum*

Parasite proteins exposed on the surface of the infected RBC	**PfEMP1, Rifins**
Proteins found on the membrane skeleton of infected RBC	**KAHRP, PfEMP3, MESA, RESA**
Altered native RBC proteins	**Band 3, glycophorin, protein 4.1**

2.2.3.1 Parasite proteins exposed on the surface of the infected red blood cells

PfEMP1 (*Plasmodium falciparum* Erythrocyte Membrane Protein 1)

PfEMP1 was firstly identified as a molecule of parasite origin exposed on the surface of the parasitized cell by R. J. Howard and colleagues in 1983 [24] and was later confirmed by Leech and coworkers (1984b) [25] using monkey red blood cells infected with *P. falciparum*. It varies in size between different parasite lines with molecular weight 250-330 kDa and is antigenically highly variable.

Synthesis of PfEMP1 begins at the late ring/early trophozoite stage. It is then transported to the RBC membrane. PfEMP1 is insoluble in Triton X-100 detergent, which indicates a link to the RBC membrane skeleton. It was shown that PfEMP1 anchors to the membrane skeleton in infected RBCs via another parasite derived protein KAHRP (Knob-associated Histidine-rich Protein) [26-28]. By the late trophozoite stage, PfEMP1 is found in association with knobs [29] and is exposed on the RBC surface. The total number of PfEMP1 molecules on the RBC surface is unknown but it is not believed to be an abundant molecule and the total may lie in the thousands.

Most or all PfEMP1 molecules contain a binding site for CD36 and some isolates are capable of binding chondroitin sulphate A (CSA).

Rifins

Rifins is a second group of parasite proteins in addition to PfEMP1, approximately 20 to 170 kDa. Like PfEMP1, the expression of rifins is parasite stage-specific and they appear on the RBC surface about 14-16 hours after invasion, as the parasites develop into mature, pigmented trophozoites [30-32].

2.2.3.2 Proteins found on the membrane skeleton of infected RBC

KAHRP (Knob-associated Histidine-rich Protein)

KAHRP was identified by comparing the stage-specific proteins of 'knobby' and 'knobless' lines of the parasite isolate FCR3 [33, 34]. The protein identified in knobby parasites by these studies is now referred to as KAHRP. It has been extensively studied because of its central importance in the changes occurring to the infected RBC, particularly with respect to the formation of the knob structure [35] and its essential role in cytoadhesion.

With molecular mass of 80 to 108 kDa, KAHRP takes part in a number of intermolecular interactions with host cell proteins including spectrin, actin and ankyrin, and with the parasite protein PfEMP1 [26, 27, 36, 37]. In addition, it was found that there was a change in localization of PfEMP1 in the absence of KAHRP, which suggested some form of direct interaction between the two proteins [36]. Altogether, these interactions are able to anchor PfEMP1 securely to the membrane skeleton and provide a stable structure that allows flowing parasitized RBCs to

cytoadhere and to resist subsequent detachment by the shear forces experienced in the dynamic environment of the circulation *in vivo*.

PfEMP3 (*Plasmodium falciparum* Erythrocyte Membrane Protein 3)

First described in 1992 [38], PfEMP3 is found at the erythrocyte membrane skeleton, both within and outside the knob structures [39]. Although it is not yet known what is its mechanism of interaction to host proteins at the membrane skeleton and whether it is linked to PfEMP1 or KAHRP, specific knockouts suggested that this protein had no direct involvement in transport or anchoring of PfEMP1 [40]. Further phenotypic analysis will be needed to determine the role of PfEMP3 in parasite biology.

Unlike PfEMP1, which is found at knobs, with most of the protein exposed extracellularly, PfEMP3 is located fairly uniformly throughout the cell, and is attached to the underside of the RBC membrane skeleton.

MESA (Mature-parasite-infected Erythrocyte Surface Antigen)

MESA is a 250-300 kDa phosphoprotein [41, 42] produced early in the trophozoite stage and found in association with the erythrocyte membrane skeleton [43, 44]. Like PfEMP3, MESA interacts with the internal aspect of the host erythrocyte membrane and is not exposed on the external surface, although in the late schizonts it becomes accessible to external surface-labeling reagents such as lactoperoxidase [41, 45]. MESA has been found to interact with protein 4.1 by a series of studies [41, 46, 47]. The binding region was recently mapped to a 30-kDa domain of protein 4.1 [48].

Both MESA and protein 4.1 are phosphoproteins and in fact protein 4.1 becomes more heavily phosphorylated in infected red blood cells [41, 46, 49].

MESA was not required for cytoadherence for formation of knobs, RBC invasion, or for lysis, as measured in static assays [47, 50].

RESA (Ring-infected Erythrocyte Surface Antigen)

RESA appears in the ring-stage parasite infection, where it was found to be associated with the periphery of the infected RBC [51], and exposed to the exterior after mild glutaraldehyde treatment [52]. This protein was actually synthesized in the mature stages of the parasite and stored in a population of dense granules in merozoites and transferred to the RBC once the invading merozoite had entered the RBC [53-55]. Interestingly, about 18-24 hours after invasion, RESA gradually disappears about the same time as MESA appears [41]. RESA was found to bind to spectrin [56, 57].

2.2.3.3 Alterations to native RBC proteins during malaria infection

Besides introducing parasite origin proteins into host RBC, *P. falciparum* infection also leads to several changes in antigenicity and arrangement of host RBC membrane proteins. Whole cell mount Electron Microscopy has detected the appearance of some electron-dense aggregates but no visible changes with respect of the overall architecture of the RBC membrane skeleton was observed [58, 59].

Band 3 proteins are specifically redistributed in the region of the knob [60]. Band 3 undergoes several modifications to give rise to forms of 240 kDa and 65 kDa, which are more reactive with anti-band 3 autoantibodies.

Using FRAP (fluorescence recovery after photobleaching) technique with a confocal microscope, recent observations [61] have shown a marked decrease in mobility of the erythrocyte membrane proteins band 3 and glycophorin during the trophozoite stage of growth. Erythrocytes infected with ring-stage parasites exhibit moderate mobility indicating that the parasite is able to modify its host prior to its active feeding stage.

Parasite-induced phosphorylation of host RBC proteins is another notable phenomenon. Protein 4.1 has been found to be heavily phosphorylated in RBCs infected with *P. falciparum* [46, 49], which could inhibit spectrin-actin interactions mediated by the protein [62]. A lesser increase in phosphorylation of band 3 was observed [49]. It was postulated that the parasite-induced phosphorylation would reduce membrane mechanical stability [2].

2.3.3.4 Rheological changes in infected RBCs

Normal RBCs high deformability comes from three main features: 1) the low viscosity of the cytoplasm (essentially just a solution of haemoglobin), 2) the high surface area to cell volume ratio, and 3) the highly viscoelastic membrane. Invasion of RBCs by malaria parasites has profound effects on all of these factors and as a

consequence the rheological properties of parasitized cells are dramatically altered [4-7, 63]. Compared with normal RBCs, parasitized cells are more rigid, less deformable and, to a certain extent, more spherocytic. It was also found that the parasite exerts considerable oxidative stress on the RBC, which can contribute to loss of membrane deformability, presumably by affecting a number of different proteins [64].

Lee *et al*. (1982) [65] used filtration techniques to probe the rheological properties of a *P. falciparum* infected RBC population. Decreased filterability was reported for clinical isolates. However, this decrease in filterability was largely influenced by the presence of the rigid, spherical parasite itself, which may occupy as much as 90% of the total volume of the RBC. Furthermore, these filtration techniques were relatively insensitive and detected measurable differences only when the parasitaemia was high. Using a rheoscope, Cranston and colleagues (1984) [4] were able to observe the flow behavior of culture-derived parasitized cells directly. The RBC elongations were measured under graded levels of shear stress.

Nash *et al*. (1989) [5] aspirated individual infected RBCs using a micropipettes with 3um diameter and measured the time and pressure required for complete aspiration of the cell. By measuring the increase in the length of a 'tongue' of RBC membrane aspirated into micropipettes, they were able to calculate the shear elastic modulus for the cell membrane. They also demonstrated a loss of deformability that was greater for RBCs infected with mature stages of parasites. This was the first time that parasite-induced changes to the mechanical properties of the RBC membrane itself,

which were not influenced by the presence of the parasite, had been quantified. There was some loss of deformability at the ring stage of infection, which was attributed to a reduction in the surface area to volume ratio and a slight rigidification of the cell membrane. Membrane rigidity was even higher for RBCs containing mature forms, although no distinction was made between trophozoites and schizonts.

2.2.3.5 Altered adhesive properties of infected RBCs

The altered adhesive properties of *P. falciparum* infected RBCs can be divided into four distinct phenotypes. Parasitized cells can adhere directly to the vascular endothelial cells – cytoadhesion. Approximately 16 h after invasion of the RBC, changes occur in the surface of parasitized RBC which render them adherent to endothelial cells [66]. The interaction of infected RBCs with the endothelial cells that line the vascular intima has the most profound implication. As a consequence of this, RBCs infected by mature parasites accumulated in the microvasculature and are notably absent from the peripheral circulation, a diagnostic feature of falciparum malaria. This phenomenon, known as sequestration, helps parasitized cells to circumvent entrapment and destruction in the spleen and maintains the microaerophilic parasites in a relatively hypoxic environment. However, in small diameter vessels of the microcirculation sequestered RBCs can perturb or completely obstruct blood flow [67], with serious vaso-occlusive consequences. Knobs have been demonstrated to be essential in cytoadhesion [35, 42]. At molecular level, infected RBCs have been shown to be capable of adhering to at least 11 different receptors that are expressed on the surface of vascular endothelial cells or in the placenta. For

endothelial adhesion, the most common interaction appears to be between PfEMP1 and CD36, with studies suggesting that most, if not all parasites can adhere to this receptor [68-73]. Using a flow-based assay to quantitatively study the adhesion properties of *P. falciparum*, infected erythrocytes, Cooke *et al*. [74] suggested a collective effect of a number of membrane skeleton-associated parasite proteins, including RESA, KHARP, PfEMP3, and probably MESA.

A second form of adhesion is rosetting, the binding of two or more uninfected RBCs around a single infected RBC [75, 76]. Both PfEMP1 and the rifins have been implicated as the parasite-encoded ligands responsible for rosetting [32, 77, 78]. Evidence suggests that PfEMP1 is the most likely candidate [78, 79]. The infected RBCs can also adhere to other infected RBCs (autoagglutination) and to dendritic cells [80]. Nevertheless, the existence of rosettes and autoagglutinates in the circulation *in vivo* remains uncertain.

2.3 Rodent Malaria

A major constraint of the study of human malaria parasites is that of host specificity. The actual causative organisms cannot be maintained in convenient small laboratory animals. The avian and simian parasites were widely used until early 1950s. The situation changed in 1948 with the first discovery and isolation of the malaria parasite that was capable of infecting laboratory rats and mice [81], named *Plasmodium berghei*.

The search continued fruitfully since then and 11 species of rodent malarias have now been identified. Out of these, four from murine rodents, i.e. *P. berghei, P. yoelii, P. chabaudi, P. vinckei*, have been shown to infect laboratory mice. This classification using enzyme variation as a basis for distinguishing has now been widely accepted by all those who work with rodent malaria parasites and further given a number of subspecies resulting in a list of ten species and subspecies in this category (Table 2.2).

Table 2.2 Species and subspecies of murine malaria parasites together with their characteristic isoenzyme forms. (Data adapted from *Malaria: Principles and Practice of Malariology*. 1989 [82])

	Characteristic enzyme forms			
Species	GPI	6PGD	LDH	GDH
P. berghei	3	1	1	3
P. yoelii yoelii	1,2,10	4	1	4
P. yoelii killicki	1	4	1	1
P. yoelii nigeriensis	2	4	1	2
P. vinckei vinckei	7	6	6	6
P. vinckei petteri	5,9	5	7	6
P. vinckei lentum	6,11	5	7,9	6
P. vinckei brucechwatti	6	6	9	6
P. chabaudi chabaudi	4	2,3,7	2,3,4,5	5
P. chabaudi adami	8	2	8,10	5

GPI Glucose phosphate isomerase
6PGD 6-phosphogluconate dehydrogenase
LDH Lactate dehydrogenase
GDH NADP-dependent glutamate dehydrogenase

The rodent malarias have received a vast amount of attention both in their own right and more importantly as models for human malarias. The use of rodent malarias have apparent advantages such as having easily maintained parasites available in cheap, well characterized small laboratory animal. Besides, rodent models will allow studies

that would not otherwise be possible, for example, investigation of genetic factors like gene knock-out experiments, the use of clones of the parasites and the use of immunologically deprived hosts. Research in malarias using rodent models can have valuable extrapolation to monkeys and human with careful consideration.

The life cycles of all the murine malaria parasites are similar and resemble those of human and other primates in all essentials. In general, the infection begins with the injection of sporozoite from the salivary glands of an infected mosquito and exoerythrocytic schizogony occurs in the hepatocytes of the liver. Merozoites from the liver invade red blood cells where they become rings and trophozoites after 24 hours. Re-invasion of the red blood cells then occurs after the schizont stage where the parasite burst out of the infected cells and the infection continues with a 24 hour periodicity. Round gametocytes are formed and these are taken up by female mosquitoes of the genus Anopheles in which sporogony occurs and sporozoites are found in the salivary glands after 10-12 days at 24-26°C [82]. Table 2.3 shows the summary of the main characteristics of the four species of murine malaria parasite.

P. yoelii, which has been used in our present work, was well described and defined by Killick-Kendrick (1974) [83]. Essentially, these are large, heavily staining parasites that preferentially invade reticulocytes although they will invade mature red blood cells particularly during the early phase of an infection. The ring stages are substantial and compact and contain pigment which is difficult to see in conventional Giemsa-stained smears. Multiple invasion is common.

Table 2.3 Summary of the main characteristics of murine rodent malaria parasites. (Data adapted from *Malaria: Principles and Practice of Malariology*. 1989 [82])

Sporogony in A. stephensi	*P. berghei*	*P. y. yoelii*	*P. v. vinckei*	*P. c. chabaudi*
Optimum temperature for development °C	22	24	21	25
Time to maturity of oocyst at 25°C (d)	12	10	12	11
Size of oocyst (µm)	45	75	55	70
Length of sporozoite (µm)	11	14	15	13
Exoerythrocytic schizogony (h)	50	50	60	53
Size of exoerythrocytic schizont (µm)	30	35	45	35
Erythrocytic schizogony (h)	24	24	24	24
Number of merozoites	8-18	12-18	6-12	4-8
Schizogony occurs at	asynchronous	asynchronous	early evening	early morning
Type of blood cell	reticulocyte	reticulocyte	mature	mature
Morphology of blood stages	berghei	berghei	vinckei	chabaudi

Rodent malaria parasites are extremely easy to isolate and to maintain in the laboratory. It can be passaged from mouse to mouse by taking a drop of infected blood into Alsever's solution or any suitable diluent and infecting it intraperitoneally or intravenously into a clean recipient. Rodent malaria parasites can also be kept for long periods in liquid nitrogen or in other suitable freezers.

2.4 Optical Tweezers (or Optical Traps) Technology

2.4.1 Trapping theory

Optical trapping of dielectric particles by a single focused laser beam was first demonstrated by Ashkin *et al*. in 1986 [84]. Small dielectric particles develop an electric dipole moment in response to the light's electric field, which in a laser beam, are subjected to two distinct types of optical force: a scattering force, acting in the

direction of propagation of the light on the particle, and a gradient force, due to the interaction of dipoles with the electric field gradient that exists in the laser beam [84]. To make an optical trap, also called optical tweezers, one simply constructs a three-dimensional light gradient by focusing a laser beam by using a lens of high numerical aperture. Near the focal zone, the gradient force is sufficient to overcome the scattering force, and the small dielectric particles are pulled toward the region of high light intensity [84].

Simple ray-optics gives an illustration of the trapping basics. Figure 2.6 (a) shows a high refraction index sphere, placed off-axis in a mildly focused Gaussian beam. A typical pair of rays “a” and “b” strike the sphere symmetrically about its center O and refract through the particle, giving rise to forces F_a and F_b in the direction of the momentum change. Because the intensity of ray “a” is higher than that of ray “b”, the force F_a is greater than F_b. Adding all such symmetrical pairs of rays striking the sphere, the net force can be resolved into two components, F_{scat}, the scattering force component pointing in the direction of the incident light, and F_{grad}, the gradient component arising from the gradient in light intensity and pointing transversely toward the high intensity region of the beam. For a particle on axis, $F_a=F_b$.

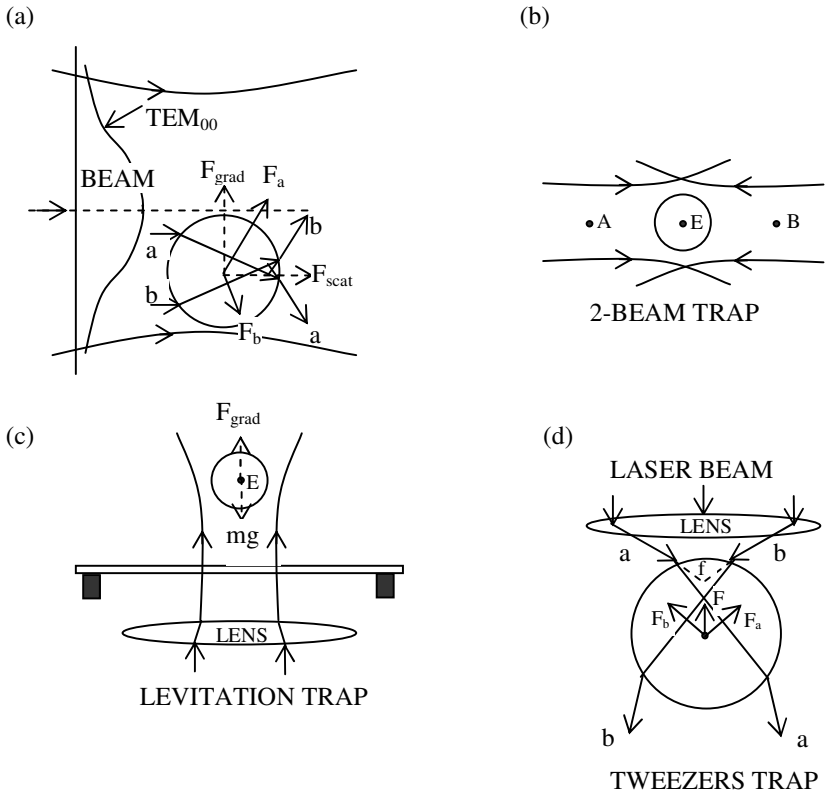

Figure 2.6 (a) F_{scat} and F_{grad} for a high index sphere displaced from TEM_{00} beam axis. (b) Geometry of 2-beam trap. (c) Geometry of levitation trap. (d) Origin of backward restoring force F for sphere located below tweezers focus f. (Adapted from Ashkin, 1997 [85].)

With understanding of the two basic force components, it is possible to devise stable three-dimensional optical traps for single dielectric particles. For example, Figure 2.6 (b) shows a trap consisting of two opposing moderately diverging Gaussian beams focused at points A and B, and the levitation trap and tweezers trap in Figure 2.6 (c, d) with single vertical beams confining a macroscopic particle where gravity and the upward scattering force balance[85]. With recent advances in electronics,

micromanipulation and laser technologies, more complicated forms such as multiple-beam optical traps have been developed [86, 87].

2.4.2 Force measurement methods

Forces exerted on trapped particles are in the piconewton (pN) range. For small displacements from the center of an optical trap, the restoring force is proportional to displacement, which means that optical trap acts like a Hookeian spring, characterized by a fixed stiffness [87]. At the edge of the trap, however, the restoring force is no longer a linear function of the displacement [88]. The trap stiffness depends on the wavelength and power of the laser used, as well as the size and refractive index of the particle, and the refractive index of the surrounding medium [84]. Theoretical prediction of trapping forces is not easy, because the equations describing light scattering in strongly convergent electromagnetic fields are difficult to solve [89]. On the other hand, several well-established methods may be used to determine trapping forces empirically, each with its own attendant advantages and disadvantages.

2.4.2.1 Escape force method

This was the first method proposed and used to estimate optical trapping forces [84]. This method is to determine the minimal force required to pull an object free of the trap entirely, usually by imposing a viscous drag force. To produce the necessary

force, the particle may either be pulled through the fluid by moving the trap relative to a stationary stage, or alternatively, the fluid can be moved past the particle by moving the stage relative to a stationary trap. For example, a trapped particle may be videotaped while translating the microscope stage at an ever-increasing rate, until the particle just escapes. The escape force can be estimated from the particle velocity immediately after escape together with the known viscous drag coefficient of the particle. This technique permits calibration of force to within accuracy of about 10%. However, this method is convenient as it does not require a position detector with nanometer resolution.

2.4.2.2 Drag force method

Within the Hookeian region of the trap, the trap stiffness α can be determined from $\alpha = F/x$, by applying a known viscous drag force, F, and measuring the displacement produced from the trap center. While holding the particle in a fixed trap drag forces are usually generated by periodic movement of the microscope stage, controlled by either triangular or sine waves [89-91]. A well-calibrated piezo stage and position detector are needed. In addition, the viscous drag coefficient of the particle must be known, which can be problematic for irregularly shaped particles. Therefore, this method is best suited to uniform spherical particles, for which explicit expressions for the drag exist, even near chamber walls [89].

2.4.2.3 Equipartition method

One simple and straightforward way of determining trap stiffness, α, is to measure the thermal fluctuations of a trapped particle. The stiffness of the traps is then computed from the Equipartition theorem for a particle bound in a harmonic potential: $1/2kT = 1/2\ \alpha\langle x^2\rangle$, where kT is Boltzmann's constant times the absolute temperature and x is the displacement of the trapped particle. The main advantage of this method is that knowledge of the viscous drag coefficient is not required and therefore of the particle's geometry as well as the fluid viscosity. However, a fast, well-calibrated position detector is essential. In addition, the analog bandwidth of the detection system as well as other systematic sources of noise and thermal motion need to be taken into consideration.

2.4.3 Applications of optical tweezers

Operating in piconewton force range, single or arrays of optical tweezers have exciting and surprising applications in micromanipulation in the microscopic world. For example, an array of traps can continuously sort fluid-borne particles, acting like a sieve[92, 93]. Spatially resolved photochemistry using optical tweezers has been used to fabricate small complex three-dimensional structures. Optical tweezers can also be used as actuators, such as the micrometer-scale hydraulic pump [94] for micromachines helping to advance the lab-on-a-chip and related technologies for medical diagnostics, environmental testing and point-of-use microfabricaton.

More interestingly, piconewtons are well matched to the kinds of forces encountered at the level of biological ultrastructure. Forces of this magnitude can move cells, bend cytoskeletal elements, such as microtubules, distort proteolipid membranes, arrest organelle movements or swimming bacteria and overcome the motion of biological motors, such as myosin, kinesin and the bacterial rotary engine. They are probably sufficient to disrupt some macromolecular bonds, such as receptor-ligand complexes.

Many recent studies have shown the utility of optical tweezers. Ashkin and Dziedzic used optical tweezers to grasp membranes inside plant cells and pull out slender viscoelastic filaments [95]. Block, Blair and Berg made a micromechanical measurement of the torsional compliance of single bacterial flagella in E. coli and Streptococcus [96]. Optical traps hold great promise in the study of motor molecules, where the forces generated by these mechano-enzymes are believed to be in the range of piconewton or so. One especially powerful approach has been to use micrometer-sized spheres as 'handles' to hold molecules or molecular assemblies. Ashkin and coworkers used optical tweezers to arrest and then release small organelles powered by attached motors in the giant amoeba *Reticulomyxa,* thereby obtaining an estimate of motor force [97]. Kuo and Sheetz undertook a related approach with latex spheres to estimate the force produced by kinesin along microtubules [98]. Also by attaching small 'handles' of microspheres to the ends of DNA made fluorescent with ethidium bromide, Chu and colleagues stretched out single molecules followed by releasing, to estimate the persistence length of the polymer [99].

As tools for biology, multifunctional optical traps will facilitate new approaches to cell sorting, macromolecular purification, intracellular surgery, embryonic testing and highly parallel drug screening as well as great many other possibilities.

2.5 Mechanical Probing of the RBCs Using Optical Tweezers

The red blood cell has a simple, axisymmetric, biconcave shape with its membrane comprising the lipid bilayer and underlying cytoskeleton network, which contains the viscous cytosol but without a nucleus. Furthermore, it is highly deformable. This entire set of unique features enables the RBC to lend itself as a convenient model system to study the mechanical behavior of single cells.

A variety of experimental techniques [100] has been established to characterize deformation of the cells, including Atomic force microscopy (AFM) [101], magnetic twisting cytometry (MTC) [102], micropipette aspiration (MA) [103], shear-flow [104] and substrate stretching [105-107]. Micropipette aspiration technique [108-110] has been most commonly used to study human RBCs, where the cell is deformed by applying a suction pressure through a micropipette placed on the surface of the RBC. By measuring the geometry changes of the cell, the elastic response of the RBC is extracted. Under appropriate control, it can also be useful in assessing the viscoelastic relaxation properties of the RBC upon release of the aspiration pressure [111]. However, there is still the need to develop new experimental techniques whereby well controlled stress states can be imposed on a single cell with high precision.

Optical tweezers are finding increasing application in the study of single biological cells. Ashkin *et al*. (1987) [112] used infrared laser beams to optically trap and manipulate single cells. An optical trap was used by Svoboda *et al*. (1992) [113] to isolate the membrane skeleton from a red blood cell, which was treated with a non-ionic detergent, so as to study the effect of ionic strength on the contraction of the spectrin network. Bronkhorst *et al*. (1995) [114] employed triple traps to deform and to explore shape recovery of red blood cells.

Direct tensile stretching of the human red blood cell using optical tweezers to extract elastic properties was first reported by Hénon *et al*. (1999) [115] who attached two silica beads non-specifically to diametrically opposite ends of the cell, trapped both beads with laser beams, and imposed tensile elastic deformation on the cell by moving the trapped beads in opposite directions. Forces were calibrated by subjecting a trapped bead to counter flow following the procedures outlined by Svoboda and Block (1994) [88] and Simmons *et al*. (1996) [116].

Stokes' law was used to estimate the force on the trapped bead from known fluid velocity. With a 1.064 μm Nd:YAG laser beam of 605 mW maximum emission power and silica beads 2.1 μm in diameter, they imposed maximum tensile forces of up to 56 pN on discocytic and osmotically swollen, nearly spherical cells. By employing simple analytical expressions based on two-dimensional linear elastic, small deformation, idealization of the cell, they examined variations in only the transverse diameter of the cell with applied force, and ignored possible contributions

to deformation arising from the bending stiffness of the cell membrane and cytoskeleton. Finite contact between the beads and the cell membrane during stretching by optical tweezers was also not considered. The in-plane shear modulus of the cell membrane was estimated from this approach to be 2.5 ± 0.4 μN/m. This estimate is lower than the range of shear modulus values of 4 to 10 μN/m obtained from a number of independent investigations which employed the micropipette aspiration technique [110, 111, 117, 118].

Sleep *et al*. (1999) [119] also estimated elastic properties of the human red blood cells by optical tweezers where two polystyrene latex beads of 1 μm diameter were trapped using a 1.047 μm Nd:YLF laser beam. In this experiment, one bead was held fixed and the other moved with a second trap to induce tensile deformation in the cell. Trap stiffness was estimated from the Brownian motion of the trapped bead. The variation of imposed force, up to a maximum of 20 pN, as a function of the transverse diameter, was reported for permeabilized spherical ghost cells whose deformation at a given force was about one half that of discocytic and osmotically swollen spherical cells. By invoking an axisymmetric cell model of Parker and Winlove (1999) [120], they estimated the in-plane shear modulus from optical tweezers studies to be nearly two orders of magnitude larger than those reported by Hénon *et al*. (1999) [115].

All of the foregoing studies of cell deformation by optical tweezers involve primarily small elastic deformation at low applied forces. However, a study by Kellermayer *et al*. (1998) [121] reported an estimated stretching force in excess of 400 pN using

optical tweezers where a 1046 nm Nd:YAG laser with a maximum power of 1.5 W was used to trap a 3 μm diameter latex bead. Studies of deformation conditions at larger strain levels inevitably require much higher forces. Some investigations have demonstrated severe stiffening of the RBC infected with *P. falciparum* by recourse to micropipette aspiration experiments [3-6]. In another study [7] on deformability of RBCs parasitized by *P. falciparum* and *P. vivax* to different developmental stages in a laminar shear flow system, mechanical deformation characteristics in the advanced (schizont) stages of erythrocytic development could not be determined because of experimental difficulties. At present, there is not yet a systematic study done on the progressive stiffening with the maturation of malaria parasite inside RBCs with direct and continuous force-displacement measurements obtained from the early ring stage to the late schizont stage. This information is essential for proper interpretation of stage-specific deformation characteristics which are conceptually feasible to obtain using the optical tweezers method. This method will further provide a possible means to investigate systematically the effects of the progression of the infestation of the red blood cell with malaria parasite, on the deformation characteristics and elastic properties of the cell membrane.

Chapter 3: Methods and Materials

This chapter describes the procedures for RBC sample preparation work, experiments to be conducted using the optical tweezers system as well as the force calibration method for this optical tweezers system. A section on the computational method to model the stretching of the RBC will also be described.

Both human and rodent RBCs have been tested. Human RBCs used were healthy blood samples obtained freshly from donors and *P. falciparum* RBCs were cultured *in vitro*. Both healthy and *P. yoelii* rodent RBCs were obtained from laboratory mice.

3.1 Human RBCs

To obtain human RBCs, blood samples from healthy adults were first obtained via finger prick using a Lancet Device (Becton Dickinson). The blood was then washed three times in phosphate buffered saline (PBS) with pH 7.4, using a centrifuge to remove the other blood components, including white blood cells. The isolated RBCs were resuspended in the same buffer solution.

P. falciparum strains *3D7* [122] was obtained by culturing them *in vitro* using known methods [123], with appropriate modifications [124]. Cultures were grown at 5% hematocrit in 25 ml tissue culture flasks in a complete medium that consisted of RPMI 1640 supplemented with 4.2 ml/100 ml 5.0% $NaHCO_3$ and 0.5% w/v albumax

(Gibco-BRL). Cultures were gassed with 3% O_2, 5% CO_2 and 92% N_2, and incubated at 37ºC in a complete medium.

3.2 Rodent RBCs

The nonlethal murine malaria *Plasmodium yoelii yoelii* 17X (a kind gift from Dr. Peter Preiser) was maintained *in vivo* in BALB/c mice. When blood infection reached a very high percentage (approximately 90%), a drop of blood was taken from the tail vein and injected intra-peritoneally into a healthy mouse. Blood stage parasites were collected from the tail vein of the infected mouse. To avoid other physiological factors which at very high parasitemias may be reasoned to affect RBC rigidity, only those with parasitemias less than 70% were used for stretch tests.

Samples of normal mouse blood were collected from the tail vein of healthy BALB/c mice.

3.3 Stretch Test Sample Preparation

All blood samples – normal human blood from finger prick, *Plasmodium falciparum* RBCs from *in vitro* culture or normal and *Plasmodium yoelii* RBCs from mouse tail vein were collected freshly and prepared on the day of experiment.

The blood sample was washed three times in phosphate buffered saline (PBS) with pH 7.4, using a centrifuge to remove culture media (for *in vitro* culture) and the other blood components, including white blood cells. Normal RBCs were centrifuged at

1500 rpm. For the malaria infected human and rodent RBCs, soft centrifugation at 1000 rpm was used to avoid damage to the diseased cells. The isolated RBCs were resuspended in the same buffer solution.

Silica beads, 4.12 μm in diameter (Bangs Laboratories, USA), were washed in PBS with pH 7.4 via centrifugation process and added to the resuspended red blood cells in PBS with pH 7.4 and stored at room temperature for 1 hour to allow for spontaneous and nonspecific binding of beads to cells. The *Plasmodium falciparum* infected human RBCs have shown markedly increased stickiness and prolonged culture will result in a large degree of coagulations among cells and silica beads. Therefore, *Plasmodium falciparum* RBCs were mixed with silica beads immediately before the optical tweezers stretch tests. Apart from this minor alteration, all samples were prepared according to the standard procedure ensuring the same experimental condition.

Prepared RBCs and silica beads mixture were diluted in a solution of PBS (pH 7.4) and 0.3 bovine serum albumin (BSA) (Sigma) and added to a 2-well chamber (Lab-Tek, Figure 3.1) for subsequent test. The addition of BSA can effectively limit the silica beads adherence to the glass bottom of the chamber.

Human RBCs of four conditions were prepared for optical tweezers stretch tests, including healthy RBCs obtained via finger prick of the donor (Hh-RBC) and exposed to *P. falciparum* but uninfected (Pf-U-RBC), and three development stages

of parasitized RBCs, being ring form (Pf-R-RBC), trophozoite (Pf-T-RBC,) and schizont stages (Pf-S-RBC).

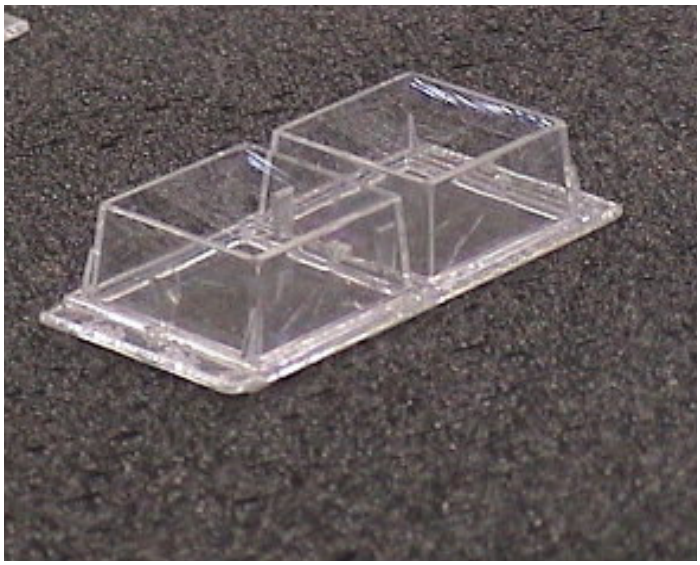

Figure 3.1 A 2-well chamber (2×2cm each) used in the present experiments.

Likewise, healthy mouse RBCs and *P. yoelii* parasitized mouse RBCs at different stages were abbreviated in consistency with the human samples as: healthy (Hm-RBC), exposed to *P. yoelii* but uninfected (Py-U-RBC), ring form stage (Py-R-RBC), trophozoite stage (Py-T-RBC), and schizont stage (Py-S-RBC).

3.4 Fluorescent Labeling

DAPI (4', 6-diamidino-2-phenylindole, dihydrochloride hydrate, Sigma) was used to label the nuclear DNA of both *Plasmodium falciparum* and *Plasmodium yoelii* invaded RBCs, in order to incorporate *in situ* fluorescent visualization during stretch

tests. This was facilitated by a fluorescent module mounted on the microscope equipped with the optical tweezers. Prior to mixing the infected RBCs with silica beads, the RBCs were incubated with 1 µg/ml DAPI in PBS at room temperature for 15 minutes.

3.5 Optical Tweezers System

The single-beam gradient optical tweezers system used in this project incorporates an inverted microscope (Leica Microsystems, Wetzlar, Germany) and a laser module (LaserTweezers, Cell Robotics, Inc.). The trapping beam is a 1064 nm Nd:YAG laser with a maximum power of 1.5 W. Focusing the laser through an oil immersion lens (100× magnification, numerical aperture 1.4) forms the optical trap. Figure 3.2 shows the experimental setup for optical tweezers stretch tests.

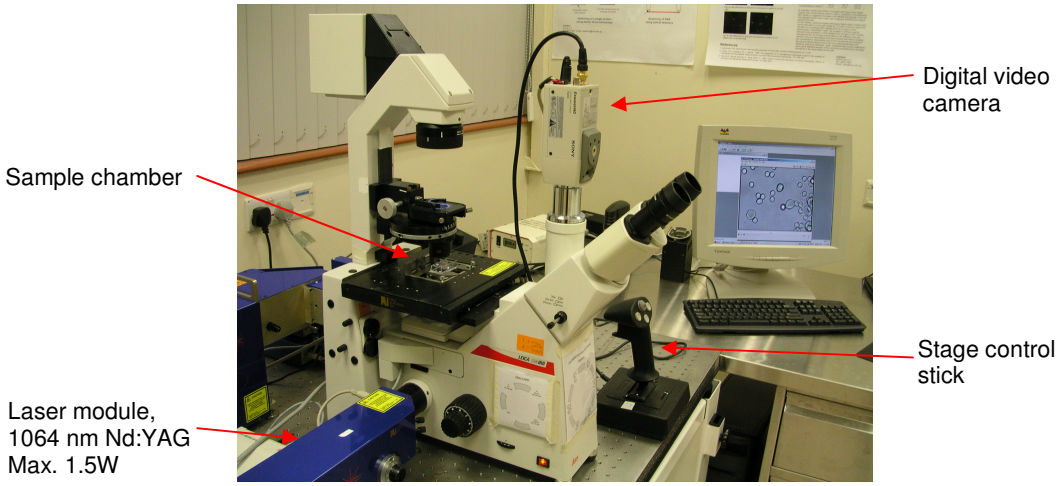

Figure 3.2 Optical tweezers system and experimental setup.

3.6 Stretch Tests

As the experiment used a single trap optical tweezers system, an individual stretch test should be conducted on a RBC with two diametrically attached beads, one of which was adhered to the glass slide and the other free for trapping as shown in Figure 3.3. For each stretching test, under different laser powers, the free bead was trapped and the sample stage was slowly translated until the bead escaped the trap. By this means, each RBC was stretched over a range of forces. All stretch tests were recorded digitally by a video camera (SONY, 30 frames/sec) for subsequent image analysis of cell deformation.

Axial diameters (in the direction of stretch) and transverse diameters (orthogonal to stretch direction) of the cell when the trapped bead just escaped the trap were measured from the still-frame image using Image Pro Plus (Media Cybernetics). The recorded videos were obtained from the bottom view of the chamber. Since the optical trap in this system was formed slightly above the focus plane, the cell was stretched at an angle to the glass slide instead of horizontally (Figure 3.3). Hence the actual axial diameter was calculated from both the projected diameter and the trapped bead height, 3μm, which was extracted from the readings of the microscope coaxial fine focus drive while lowering the trap from its normal position to where the focus plane was.

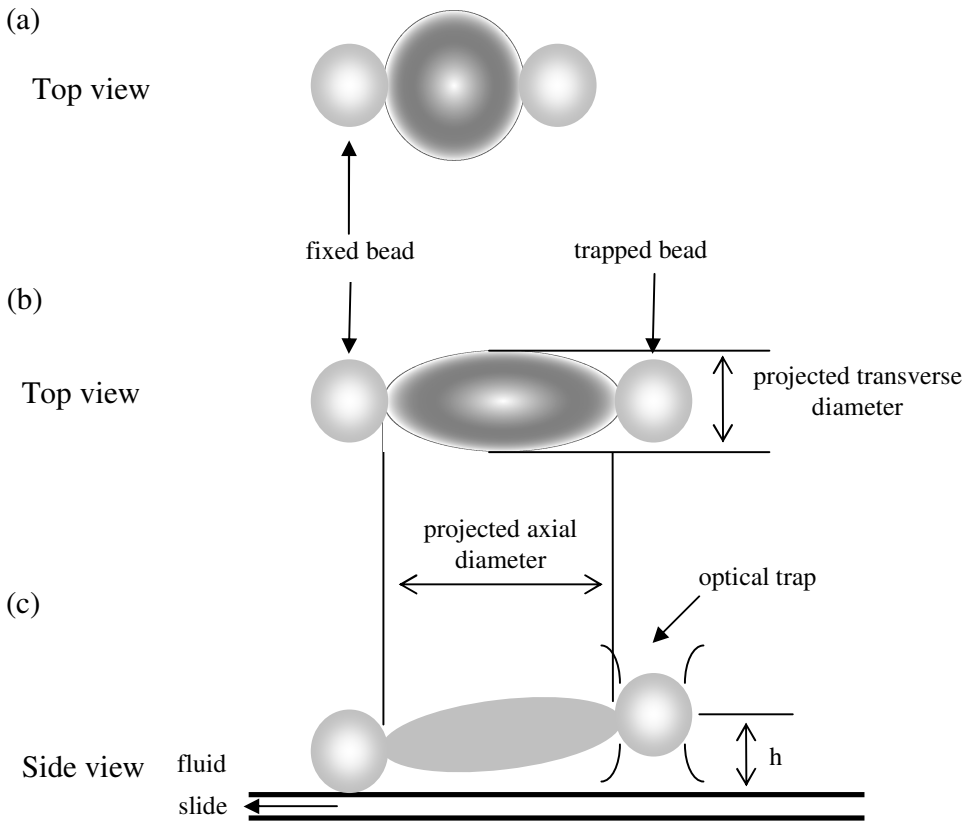

Figure 3.3 Illustration of an optical trap method for cell stretching. (a) Top view of a RBC with two silica beads, each 4.12 μm in diameter, non-specifically attached diametrically across the cell. One of the beads (left) is anchored to the surface of the glass slide. (b) Top view and (c) side view of a RBC undergoing stretching. While the trapped bead remains stationary, moving the slide stretches the cell. The trapped bead is at a height h from the glass slide.

3.7 Force Calibration

Because cell deformations were measured at the point when bead escaped from the trap, the optical tweezers system was calibrated using an escape force method [88]. In this technique, the force required to dislodge a trapped bead was calibrated against

a known viscous drag force. The calibration procedure involved trapping a silica bead in the working solution, PBS and 0.3% BSA, at a measured height, h = 3 μm, above the glass slide surface. The fluid and height of the trapped bead from the slide surface were kept unchanged throughout calibration and mechanical deformation. As the microscope stage was translated, the fluid exerted a viscous drag force on the trapped bead, as shown in Figure 3.4. The viscous drag force equals the trapping force when the bead just escapes the trap. From the stage velocity, v, at the point of escape of the trapped bead, the drag force, which is the opposite of the escape force, was estimated as

$$F=\beta v. \qquad (1)$$

The viscous drag coefficient β for a spherical bead located near a wall was described by Faxen's Law [88],

$$\beta = \frac{6\pi\eta r}{1-\frac{9}{16}(r/h)+\frac{1}{8}(r/h)^3-\frac{4}{256}(r/h)^4-\frac{1}{16}(r/h)^5}, \qquad (2)$$

where, for the present experiments, the bead radius r = 2.06 μm, height of the bead above the wall h = 3 μm, and fluid viscosity η = 0.0013 Pa·s. Notice that Eq. (1) takes the form of Stokes' law, $F = 6\pi r\eta v$, for a bead located far from the wall.

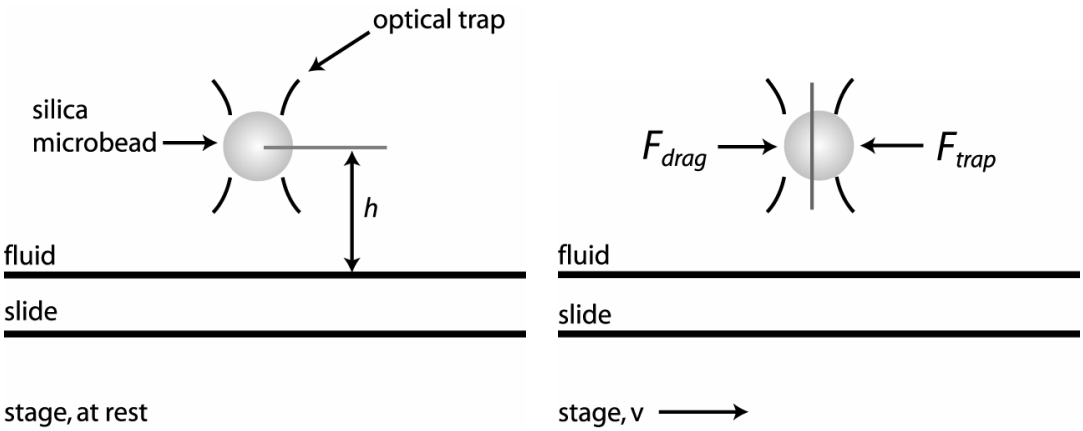

Figure 3.4 Calibration of the optical trap using an escape force method [88]. A silica bead, 4.12 µm in diameter, is trapped in fluid (PBS and bovine serum albumin, BSA) at a measured height, h = 3 µm, above the slide surface. As the microscope stage and fixed slide are translated, the fluid exerts a viscous drag force on the trapped bead. When the viscous drag force is just equal to the escape force, the bead will escape the trap.

The stage-movement technique described here differs somewhat from the fluid-chamber technique used in a related work earlier [125, 126]. The fluid-chamber technique imposed a viscous drag force by flowing fluid through a narrow channel where a bead was trapped. Fluid velocity, estimated by tracking the speed of untrapped beads, was used with Eq. (1) to determine the escape force. However, this method is limited for several reasons. Firstly, untrapped beads used to determine fluid velocity should be flowing at the same height above the slide as the trapped bead. Usually, untrapped beads flow along the surface of the slide, making fluid velocity estimates difficult. Secondly, steady fluid flow is difficult to achieve for the lowest flow rates. Thirdly, the scatter in calibration results is considerably greater than for

the stage-movement technique. The stage-movement technique, used in the current study, provided a more accurate method to determine the velocity of the fluid from known stage velocity, thereby resolving the first two limitations of the fluid-chamber method.

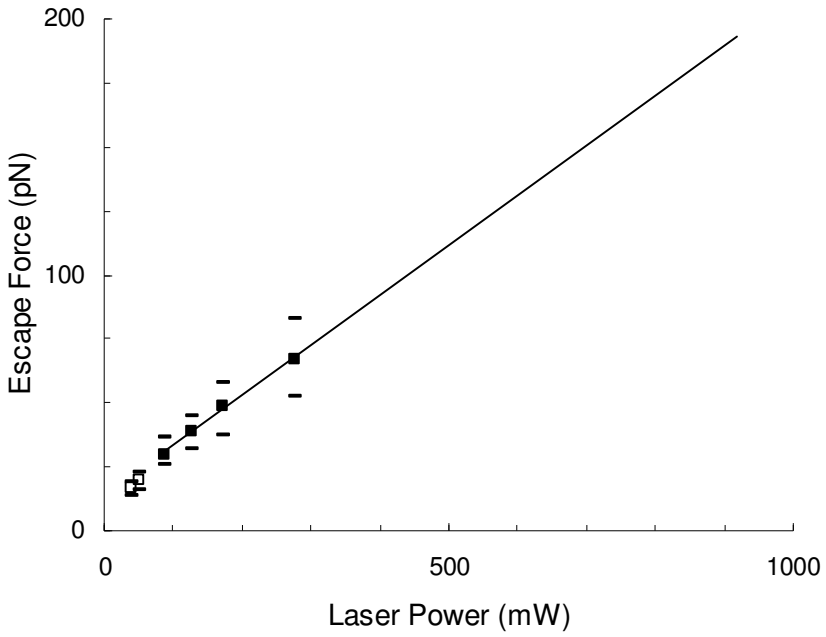

Figure 3.5 Force calibration plot showing the variation of trapping force with laser power for a 1.5 W diode pumped Nd:YAG laser source for a single optical trap system. Non-linear trends below 80mW laser power are not used for extrapolation.

The escape force over a range of laser power is shown in Figure 3.5. The reported laser power was measured at the objective lens using a power meter. At maximum power for the 1.5 W laser, only 917 mW of laser power was measured due to losses through the optics. In the current system, the stage velocity limited direct calibration to a laser power of only about 300 mW. The escape force for values of higher laser power was linearly extrapolated from the calibration data in Figure 3.5. At maximum

laser power, corresponding to 917 mW, an escape force of 193 ± 20 pN was predicted. The linear relationship between laser power and escape force was consistent with theoretical predictions [89] and empirical findings [88].

3.8 Computational modeling of RBC

A full three-dimensional computational simulations of discocyte RBC stretched by optical tweezers were used to extract the average elastic properties of the healthy, exposed and infected RBCs. Computational simulations were performed using methods adapted here with appropriate modifications from those described elsewhere [88, 125] for healthy RBCs. A two-parameter third-order hyperelasticity formulation [111] was used to model the large deformation stretching of the cell, with the strain potential energy defined as

$$U = \frac{G_0}{2}\left(\lambda_1^2 + \lambda_2^2 + \lambda_3^2 - 3\right) + C_3\left(\lambda_1^2 + \lambda_2^2 + \lambda_3^2 - 3\right)^3, \quad (3)$$

with the assumption of incompressibility (constant volume). Here G_0 is the initial value of bulk shear modulus, and λ_i (i = 1-3) are the principal stretches. The incompressibility condition implies that $\lambda_1\lambda_2\lambda_3 = 1$. In the computations, values of the parameter C_3 were taken to be those which best match experimental data ($C_3 = G_0/20$ throughout the current study). The potential function U defines the nonlinear elastic stress-strain behavior. When the initial membrane thickness is h_0, the constitutive description of Eq. (3) results in the initial in-plane membrane shear modulus $\mu_0 = 0.75G_0h_0$. The in-plane shear modulus μ of such a hyperelastic model characteristically stiffens when the uniaxial stretching strain is larger than 50%.

To perform simulations that match the averaged response of RBCs in terms of axial and transverse diameters at different erythrocytic development stages, the initial cell diameter was chosen to be approximately the averaged initial cell size; the initial maximum diameter of the biconcave cell was chosen to be 7.0-7.8 μm for the healthy, exposed but uninfected, ring form infected and trophozoite infected RBC cases. The diameter of contact between the cell surface and the silica beads was taken to be 2 μm, based on experimental observations. For the schizont RBC, an initially spherical shape with a diameter of 7 μm and a contact diameter of 1.5 μm were assumed. The in-plane shear modulus values, μ, used in the simulations was the average values extracted from finite element simulations where the choice of the modulus enabled matching of computational results of the complete force-displacement curves and contact geometry to match experimental observations. The bending modulus was chosen to be a single fixed value of 2×10^{-19} N·m, based on literature values [125]. Parametric studies at the continuum and spectrin levels indicate that the results are significantly less sensitive to the choice of bending modulus than to the in-plane shear modulus, consistent with earlier findings [127]. The three-dimensional model used here is shown in Figure 3.6. The computational simulations involve the hyperelastic deformation model for the effective cell membrane comprising the phospholipid bilayer and the spectrin network, and a fixed volume of cytosol inside the discocyte cell. A fully three-dimensional model of the biconcave cell was constructed using an averaged shape estimated from experiment [128, 129]. Because of symmetry of deformation during stretching by optical tweezers, only one half of the three-dimensional cell was simulated using symmetric boundary conditions with 12,000

three-dimensional shell elements in the finite element program, ABAQUS (ABAQUS Corporation, Pawtucket, Rhode Island, USA). The predictions of mechanical response using the foregoing continuum formulations were also found to be consistent with spectrin-level computational simulations [129].

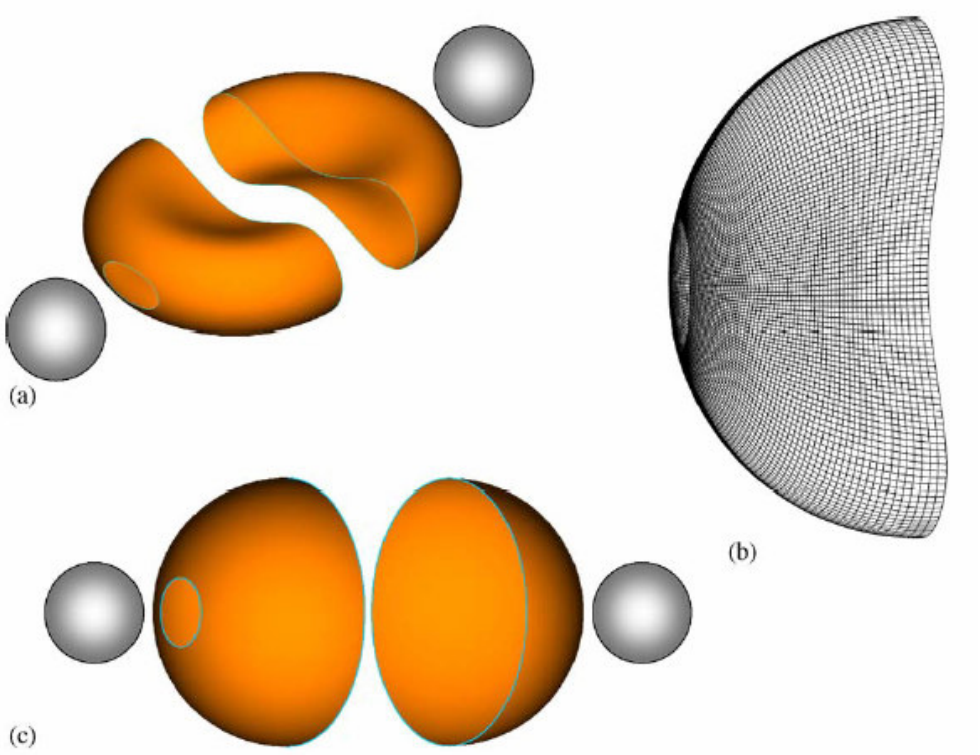

Figure 3.6 Finite element model setup of the three-dimensional geometry of the human red blood cell. (a) Original shape of the three dimensional biconcave model. The rigid silica beads were assumed to be attached to the cell over a small oval region with a diameter between 1 and 2 µm. Only half of the red blood cell was modeled because of symmetry. (b) Original mesh design of the biconcave model, where 12,000 three-dimensional shell elements were used in the simulations. (c) Companion axisymmetric spherical model. The silica beads were assumed to be attached to the cell over a small circular region with a diameter between 1 and 2 µm. The cytosol can be electively modeled as a hydraulic fluid. (Adapted from our previous work [125])

Chapter 4: Mechanical Probing of Human and Rodent Red Blood Cells Using Optical Tweezers

This chapter presents the results and discussion of this study and is arranged into three sections. In the first two sections, optical tweezers stretching tests on human and rodent RBCs are first presented. In each section, stretch data from healthy and malaria infected RBCs are compared and effects of malaria infection on RBC deformation properties are investigated. In the third section, results of a new approach combining fluorescence capability with mechanical probing are presented.

The complete test data and selected video images of stretch tests are given in the supplementary material in the form of a CD-ROM.

4.1 Stretch Tests for Human RBCs

4.1.1 Stretch tests for human normal RBCs

Figure 4.1 is the optical micrographs of one normal RBC being stretched by the optical tweezers. Two silica beads, about half the diameter (4.12 μm) of the RBC, were attached to the cell diametrically opposite to one another through nonspecific binding. One of them was adhered to the glass slide and the other one free to be trapped by the optical tweezers. When the RBC was at rest (Figure 4.1 (a)), the biconcave disc-like shape of the cell was clearly seen. While being stretched by a tensile force of 193 pN, the red blood cell underwent large deformation to nearly twice its original diameter and the central concave elongated forming a narrow fold along the central line of the cell (Figure 4.1 (b)).

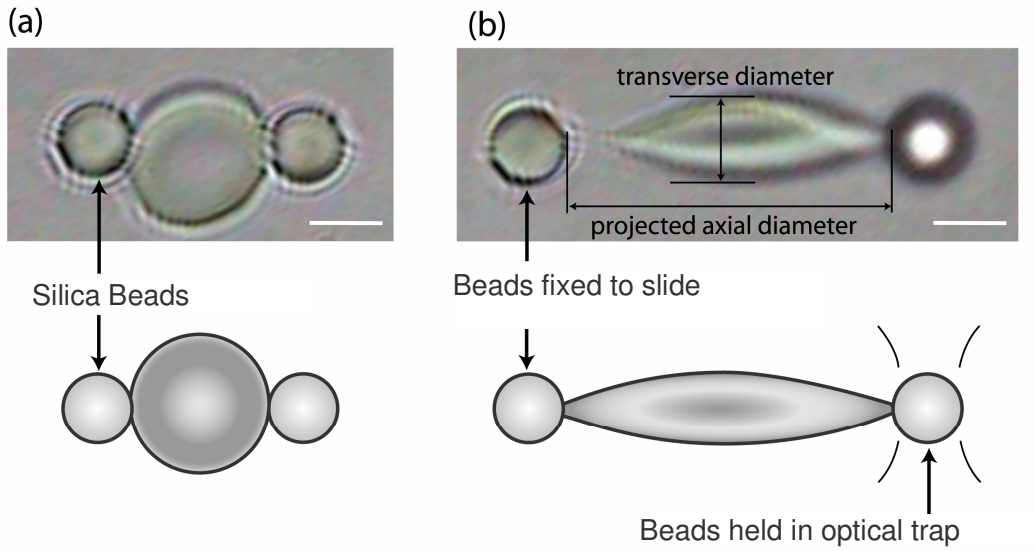

Figure 4.1 Demonstration of the optical trap method for cell stretching. Two silica beads, each 4.12 μm in diameter, are non-specifically attached to the red cell at diametrically opposite points. (a) The left bead is anchored to the surface of the glass slide. The optical image corresponds to the unstrained configuration. (b) The right bead is trapped using the optical tweezers. While the trapped bead remains stationary, moving the slide and attached left bead stretches the cell. The optical image shows an example of large deformation of a cell at 193 pN of force. Scale bar: 4 μm

By means of changing the laser power, each RBC was subjected to stretch test at 12 force levels, ranging from 16.4 pN to 193 pN. Variations in both axial and transverse diameters were quantified by image analysis. Stretch test data from 16 different RBCs from two donors were plotted as force deformation curves (see Figure 3.3 for the measurement of cell diameters). Figure 4.2 (a) shows these variations in diameters and Figure 4.2 (b) shows the percentage changes. There is no discernible difference between the normal RBCs from these 2 donors in terms of their response to optical tweezers stretching.

(a)

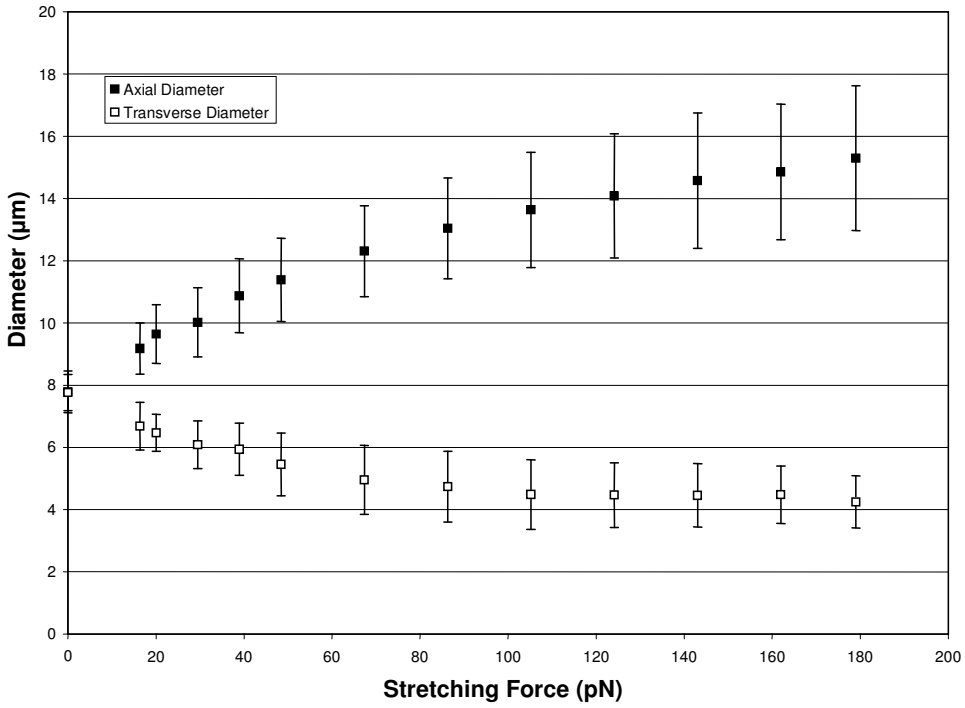
Axial Diameter
Transverse Diameter
Diameter (μm)
Stretching Force (pN)
0
2
4
6
8
10
12
14
16
18
20
0
20
40
60
80
100
120
140
160
180
200

(b)

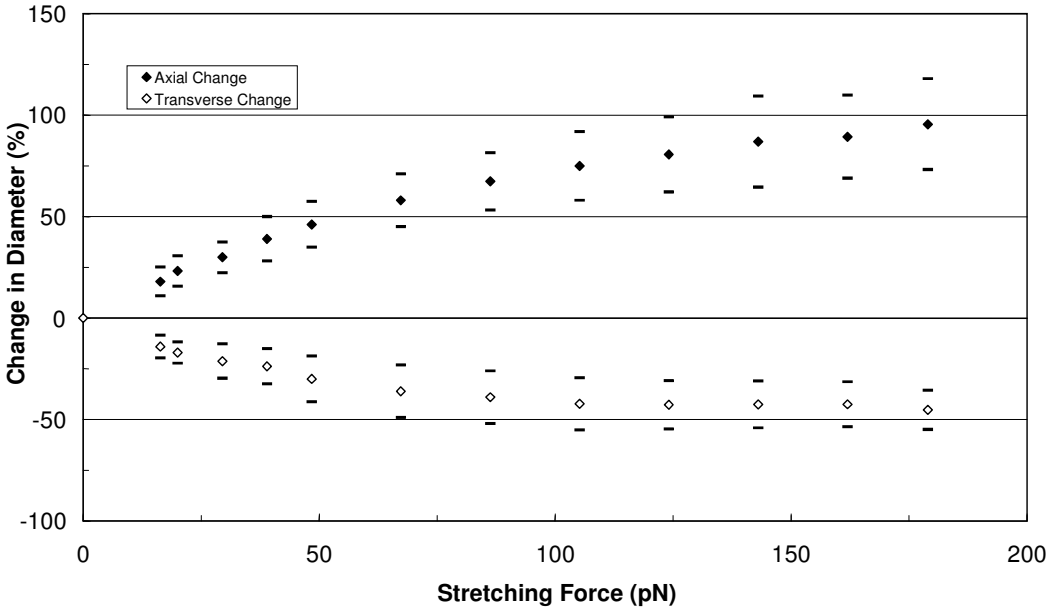
Axial Change
Transverse Change
Change in Diameter (%)
Stretching Force (pN)
150
100
50
0
-50
-100
0
50
100
150
200

Figure 4.2 (a) Variation of measured axial and transverse diameter of healthy human red blood cell against stretching force of optical tweezers during large deformation. (b) Percentage changes in axial and transverse diameter against stretching force of the same test data in (a).

The average from these stretch data shows the nonlinear stretching of normal RBCs. At 193 pN, the axial diameter of the cell increases by 95% and the transverse diameter reduces by 45%.

See supplementary material CD-ROM for the complete test data and selected stretch videos of healthy human RBCs.

4.1.2 Stretch Tests for Plasmodium falciparum Infected Human RBCs

Plasmodium falciparum infected human RBCs at three development stages were tested, including 5 ring form stage (Pf-R-RBC), 5 trophozoite stage (Pf-T-RBC) and 23 schizont stage (Pf-S-RBC) infected cells. The two control conditions were healthy (Hh-RBC, n=7) and exposed to *Plasmodium falciparum* but uninfected (Pf-U-RBC, n=8). All RBCs from the five groups were from the same donor.

Figure 4.3 shows optical images of the healthy RBC, the exposed but uninfected RBC and RBCs showing the *P. falciparum* parasite at different stages of erythrocytic development. No differences could be identified between the appearances of Hh-RBCs and Pf-U-RBCs. The ring-like structure in the Pf-R-RBC occupies a relatively small volume inside the cell. As the parasite matures, the size of the parasite and that

of the pigmented region increase with concomitant development of knobs on the cell membrane in the Pf-T-RBC and Pf-S-RBC cases. At schizont stage, the RBC is nearly dominated by the parasite vacuole and losing its biconcave shape.

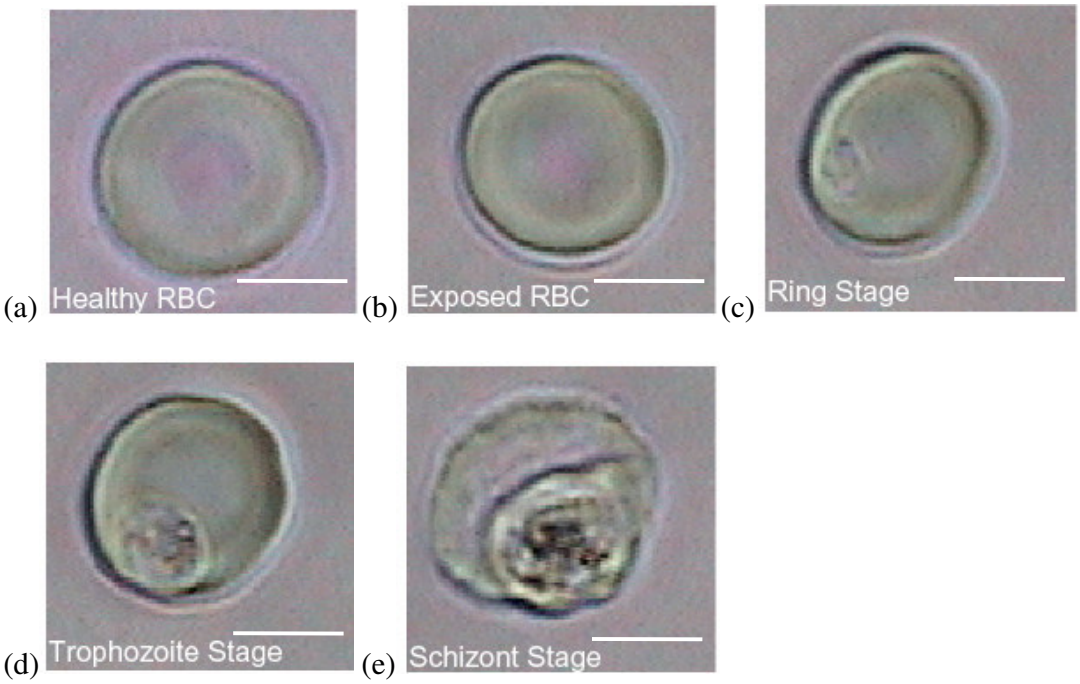

Figure 4.3 Optical micrographs of (a) healthy (b) exposed to *P. falciparum* but uninfected, and *P. falciparum* parasitized human RBCs at (c) ring stage, (d) trophozoite stage and (e) schizont stage. Note the presence of the parasite in the infected cells. Scale bar: 4 μm

Results from the stretch tests for all five groups of RBCs were compiled and plotted in Figure 4.4. Consistent with the previous section, the healthy RBCs were able to stretch to almost twice their original diameter. In comparison, the ability of a *P. falciparum* infected RBC to stretch is progressively reduced both in axial and

transverse directions as the parasite matures within the host cell. In the late infestation of schizont stage parasites, the host red cell does not exhibit appreciable deformability even at the maximum stretching force of 193 pN. In the data shown, similar scatter levels were observed for the healthy as well as infected cells.

See supplementary material CD-ROM for the complete test data and selected stretch videos of *P. falciparum* infected human RBCs.

(a)

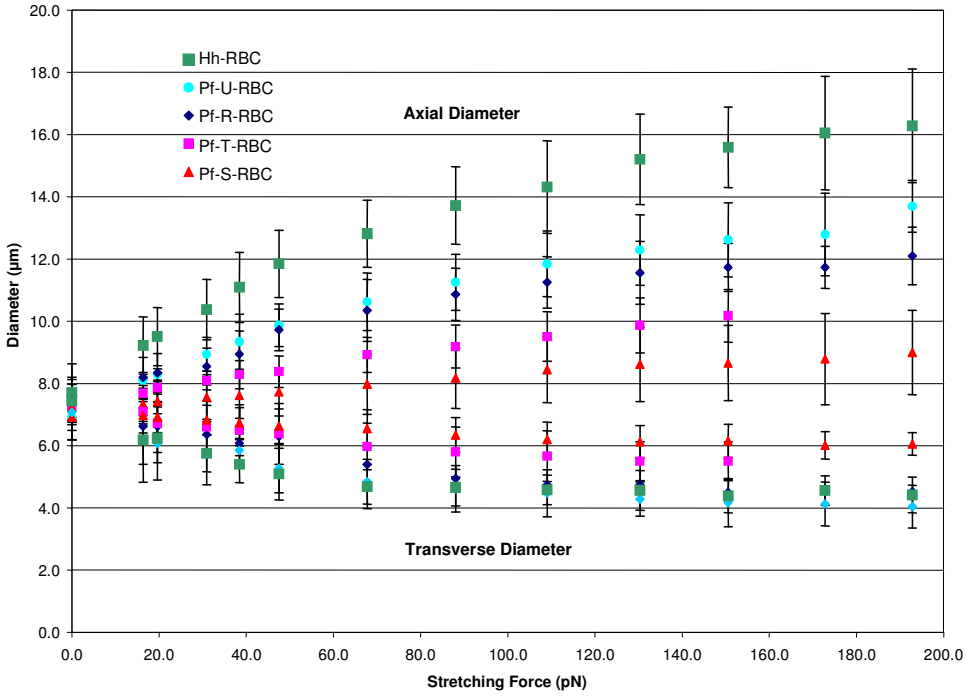

(b)

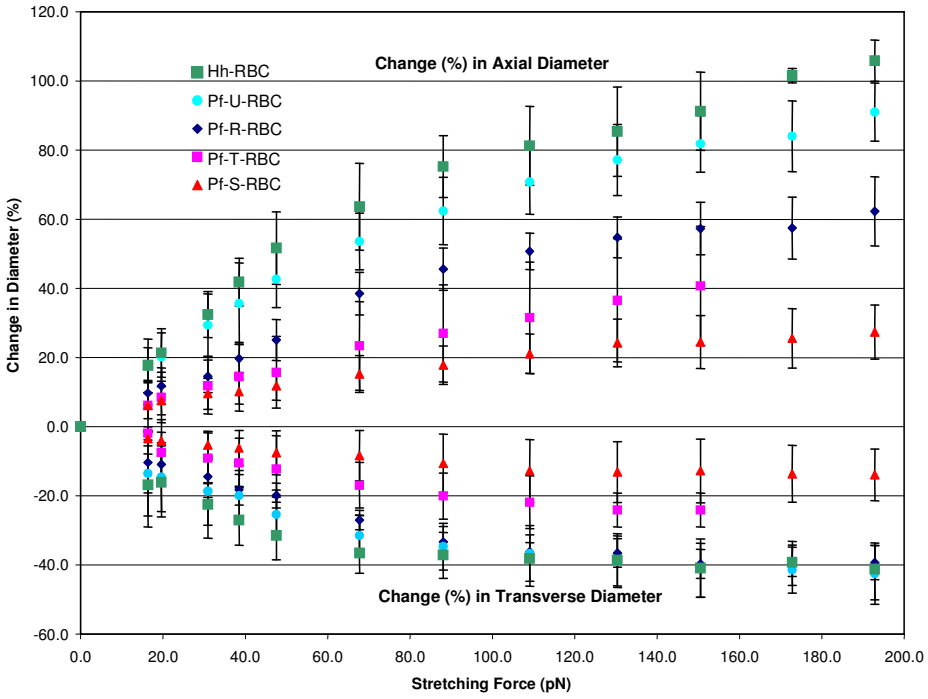

Figure 4.4 Force-deformation curves of healthy, exposed, and *P. falciparum* infected RBCs stretched by optical tweezers. The vertical bars indicate scatter estimated by standard deviation of results from multiple repeat experiments. (a) Variations of axial and transverse diameter against stretching force. (b) Percentage change in axial and transverse diameter against stretching force.

4.1.3 Three-dimensional Computational Simulations

The differences in deformability of the control groups and various developmental stages of *P. falciparum* in the RBC are clearly illustrated in three-dimensional computational simulations along with the optical micrographs (Figure 4.5) at two different force levels, 109 ± 15 pN and 193 ± 20 pN. It is evident that at both load levels, the propensity for deformation decreases significantly from the Pf-R-RBC to

the Pf-T-RBC to the Pf-S-RBC stages, where the presence of the mature parasite inside the cell can be seen.

(a)

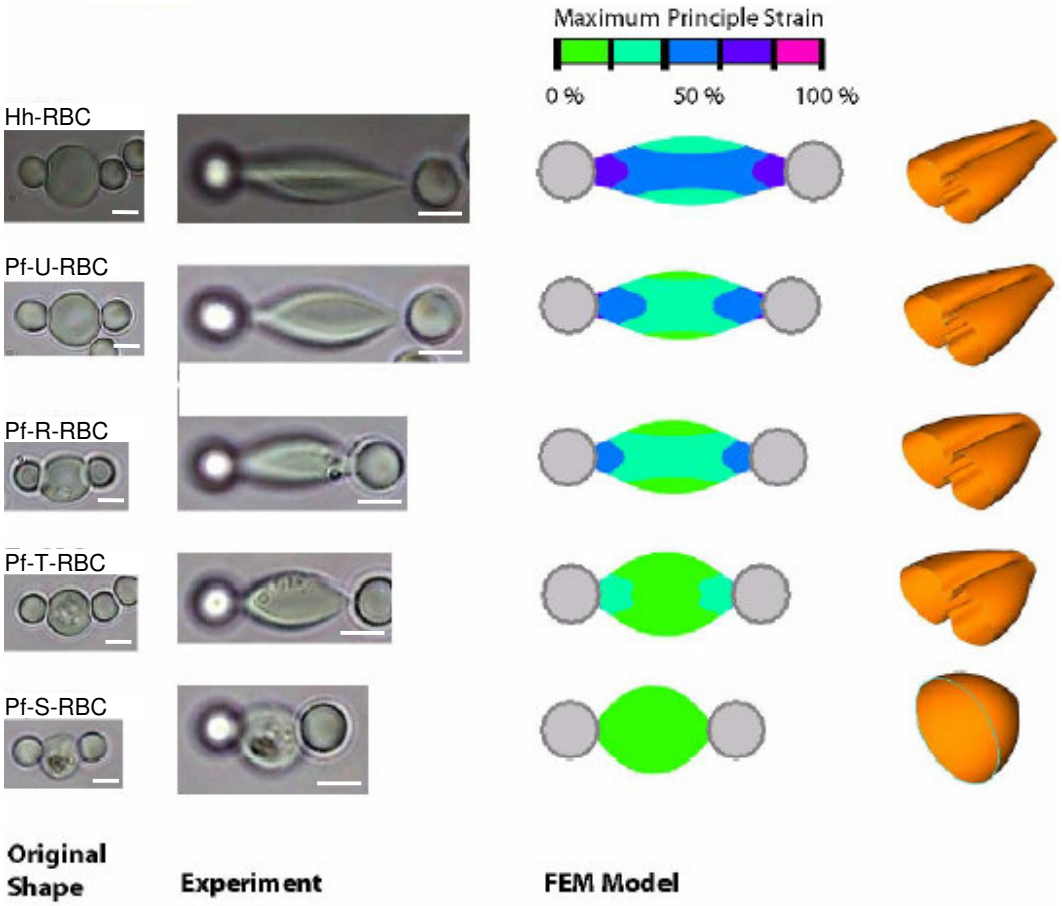

(b)

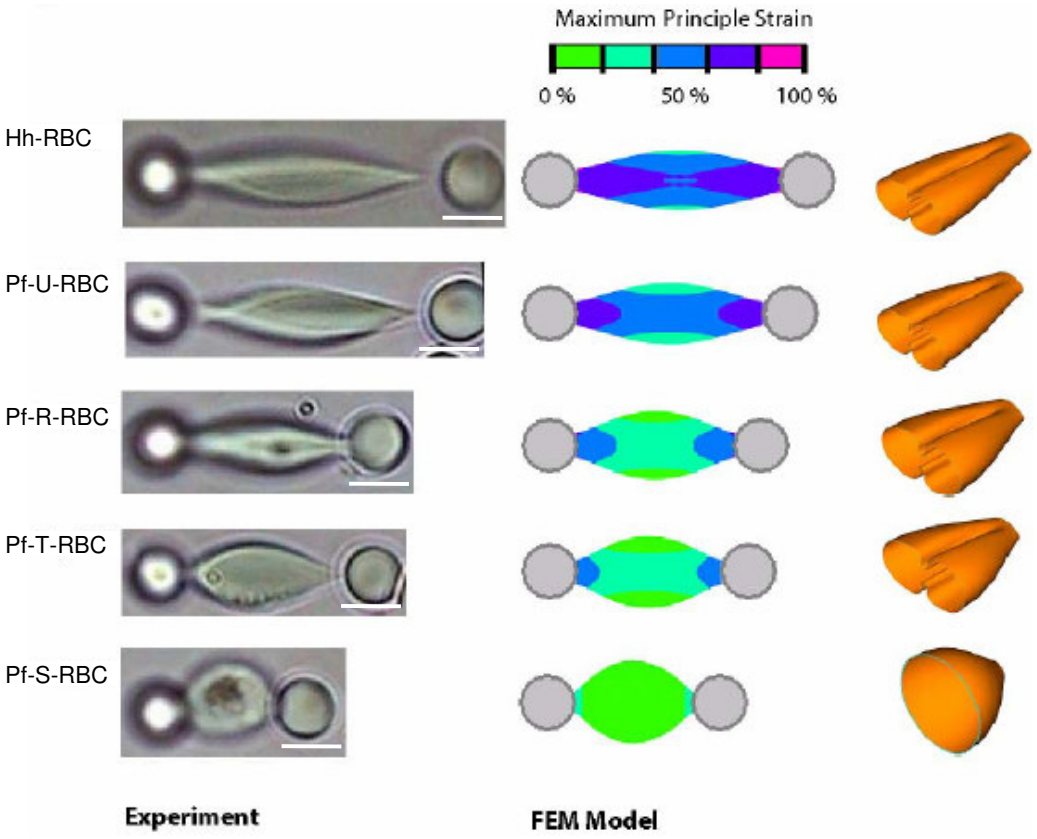

Figure 4.5 Experimental observations and computational simulations showing the effects of parasitization on RBC deformability. (a) Fixed stretching force of 109 ± 15 pN. The optical micrographs show images of cell deformation in the undeformed reference configuration as well. (b) Fixed stretching force of 193 ± 20 pN. In both figures the color contours in the central plan view show predicted distributions of constant maximum principal strain at a fixed force for the different culture stages. The extreme right column in both figures shows predicted three-dimensional shapes of one half of the deformed RBC. Scale bar: 4 μm

The extent of deformation at the higher load level is also noticeably higher for all the cases except Pf-S-RBC where no significant deformation occurs even at the stretching force of 193 pN. The middle column in these two figures shows plan views

of the stretched cell with contours of constant maximum principal strain for all the culture conditions. The right columns are three-dimensional views of the deformed shapes of one half of the cell geometry at both load levels, as obtained computationally. Note that large deformation stretching is also found to cause membrane folding, as seen in the right column images of stretched half RBCs. While the Pf-R-RBCs and Pf-T-RBCs are capable of some membrane folding despite their limited deformability, no such folding is predicted for the Pf-S-RBCs.

Table 4.1 Estimated values of stage-specific elastic modulus of parasitized RBCs.

Developmental stage	Number of cells tested	Median value of in-plane shear modulus, μ (μN/m)	Range of values of in-plane shear modulus, μ (μN/m)
Healthy (Hh-RBC)	7	5.3	4.0-7.3
Exposed, but uninfected (Pf-U-RBC)	8	8.0	6.0-10.7
Ring stage infected (Pf-R-RBC)	5	16.0	12.7-21.3
Trophozoite stage infected (Pf-T-RBC)	5	21.3	16.0-32.0
Schizont stage infected (Pf-S-RBC)	23	53.3	33.3-100.0

The values of in-plane shear modulus of the control conditions and the infected cells, obtained by matching the three-dimensional computational results with the experimental observations shown in Figures 4.4 and 4.5, are listed in Table 4.1. The Pf-U-RBCs show a very small increase in modulus compared to the value of 5.3 μN/m for the Hh-RBCs. However, the average shear modulus values for the Pf-R-RBC, Pf-T-RBC and Pf-S-RBC are 12, 16 and 40 μN/m, respectively. Late

developmental stages of *P. falciparum* are thus seen to stiffen the infected RBCs by as much as a factor of ten compared to healthy cells.

4.1.4 Discussion

Mechanical response of RBCs has long been the interest of numerous cell mechanics studies using various cell deformation methods, as reviewed previously [108-110]. Micropipette aspiration [5] and laminar shear flow [4, 6] have also been employed to probe the abnormalities in the mechanical properties of RBCs caused by *Plasmodium falciparum*. The results established here provide additional opportunities for the applications of the optical tweezers technique for the study of single cell mechanics.

There are earlier studies which used single- or multiple-beam optical traps to directly manipulate RBCs [130] or induce RBC deformation [114]. A potential drawback is the local heating of the specimen from a tightly focused laser source [131]. The use of infrared laser (1064 nm) has been shown to have minimized damage to the biological specimen [132]. However, in the present experimental observations, the healthy human RBCs will exhibit discernible impairs after prolonged exposure to the 1.5 W laser (1064 nm Nd: YAG), and about 2 minutes is enough to damage some infected RBCs. Therefore, the use of silica beads as “handles” is crucial in optical tweezers induced cell deformation studies. It has been shown that silica beads and human RBCs are able to be attached to each other through nonspecific interactions [133]. Furthermore, in our studies, it is noticed that the bonding of the silica beads to the *Plasmodium falciparum* infected red blood cell membrane was naturally enhanced

because of the increased adhesion of infected RBCs, facilitating the bonding of silica beads to cell membrane.

4.1.4.1 Comparison with previous optical tweezers studies

The in-plane shear modulus μ = 4.0–7.3 μN/m for healthy RBCs obtained in this investigation are comparable to the range of 4.0–10 μN/m reported in the literature where the estimates have been principally based on micropipette aspiration experiments. These values are also more in line with expectations than those derived from the earlier optical tweezers studies of Hénon *et al*. (1999) [115] and Sleep *et al*. (1999) [119] for small elastic deformation, possibly indicating effects of calibration methods as well as the linear elastic analysis of the data may have influenced the inference of elastic properties extracted from these optical tweezers experiments.

4.1.4.2 Comparison with micropipette aspiration and laminar shear flow studies

Prior methods based on micropipette aspiration and laminar shear flow have been employed to probe the stiffening of RBCs parasitized by *Plasmodium falciparum* [3, 4, 6, 7]. However, they were incapable of capturing the elastic deformation characteristics of the RBC schizont stage infection because of enhanced cell rigidity and increased cell adhesion. The experimental data presented here using optical tweezers method provide continuous force-deformation curves (Figure 4.4) for different erythrocytic developmental stages of *Plasmodium falciparum* invaded RBCs, indicating significant stiffening of the RBC with the maturation of the parasite from the ring stage to the trophozoite stage and finally to the schizont stage. This result

further provides quantitative information on the significant reduction in the strains induced in the RBC at the imposed force levels as a function of the maturation of parasite. There is evidence suggesting that exo-antigens released from mature parasites which have not invaded the RBCs could increase the stiffness of exposed but uninfected RBCs [4, 134]. Consistently, our experiments did show that the average stiffness of Pf-U-RBC is 8.0 μN/m compared to the value of 4-5.3 μN/m for Hh-RBCs (Figure 4.4). With the appropriate choice of the in-plane shear modulus, for a fixed value of the bending modulus of the cell membrane, our computational simulations lead to a good match between predicted and experimentally observed variations in axial diameter, transverse diameter, contact diameter and overall shape (Figure 4.5).

It has been predicated primarily based on micropipette aspiration, that the elastic modulus of the human RBCs can increase approximately three-fold from *P. falciparum* infection [3-6]. Systematic experiments [3] have shown that knob-associated histidine-rich protein (KAHRP), which associates with spectrin, actin and ankyrin in the RBC cytoskeleton, contributes significantly to the increase in RBC membrane rigidity by possibly cross-linking with the spectrin. Such interactions and the anchoring of KAHRP with the *P. falciparum* erythrocyte membrane protein 3 (PfEMP3) could lead to increases in modulus by 50% or more, based on a particular parasitic strain and time of culturing.

Additional contributions to the stiffening of RBCs by the intracellular parasite could arise from alterations to the hemoglobin structure and cytosol volume. The RBC infected with the parasite at schizont stage undergos a shape change to a sphere compared to the biconcave shape of a healthy RBC, which will lower the surface to volume ratio and consequently weaken the deformability.

The current work demonstrates the feasibility of reproducibly and accurately tracking the progressive decrease in the large elastic deformation of the infected RBC in a quantitative manner under a well-controlled stress state. Our results imply an order of magnitude increase in the effective shear modulus of the parasitized RBC, with the possibility of a greater contribution to stiffening from changes to the cytoskeletal network than previously anticipated [3-7]. Figure 4.6 shows a comparison of the mechanical properties of the malaria-infected RBCs obtained in the work with those estimated previously from micropipette aspiration measurements [3] and laminar shear flow method [7] for the early developmental stages of the parasite. Estimates of elastic modulus from optical tweezers stretching of healthy cells are comparable to those from other methods. Whereas it is evident that the present experiments indicate significantly greater stiffening in the ring stage, trophozoite stage as well as schizont stage than previously determined, possibly as a result of its greater flexibility to circumvent experimental artifacts associated with membrane stiffening and increased cell adhesion.

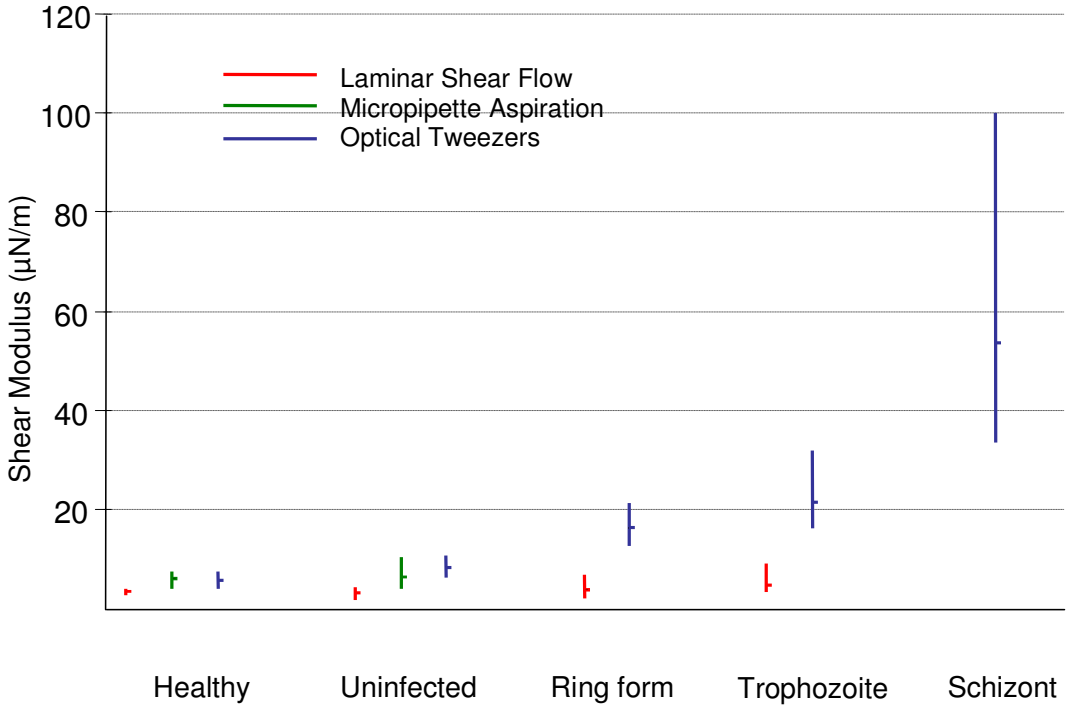

Figure 4.6 A comparison of the RBC stiffening response estimated from optical tweezers for the ring stage, trophozoite stage and schizont stage of erythrocytic development of *Plasmodium falciparum* with available results based on micropipette aspiration [3] and laminar shear flow [7] methods.

4.2 Stretch Tests for Rodent RBCs

4.2.1 Results

Infections of BALB/c mice with nonlethal *Plasmodium yoelii* 17X revealed all erythrocytic stages in peripheral blood. This is presumably due to the lack of infected RBC sequestration in this mouse model. In contrast, virulent lines such as *P. yoelii* 17XL do exhibit some sequestration of infected RBC in cerebral vasculature [135].

Micrographs of normal and *P. yoelii* infected mouse RBCs at different stages are shown in Figure 4.7. While a normal mouse RBC is about 6.8 µm in diameter, the infected cells are perceptibly larger than normal ones. The enlargement of infected RBCs is more discernible while the infection progress within the host cell. In later stage of parasitization namely schizont, the average cell diameter increased by 10.1% (Table 4.2). One of the main characteristics of the blood stage *P. yoelii* parasite is its predilection for reticulocytes, the immature RBCs, which are slightly larger in size than the more mature ones [82, 136]. Polyparasitism is common to the *P. yoelii* species, which might also result in cell enlargement.

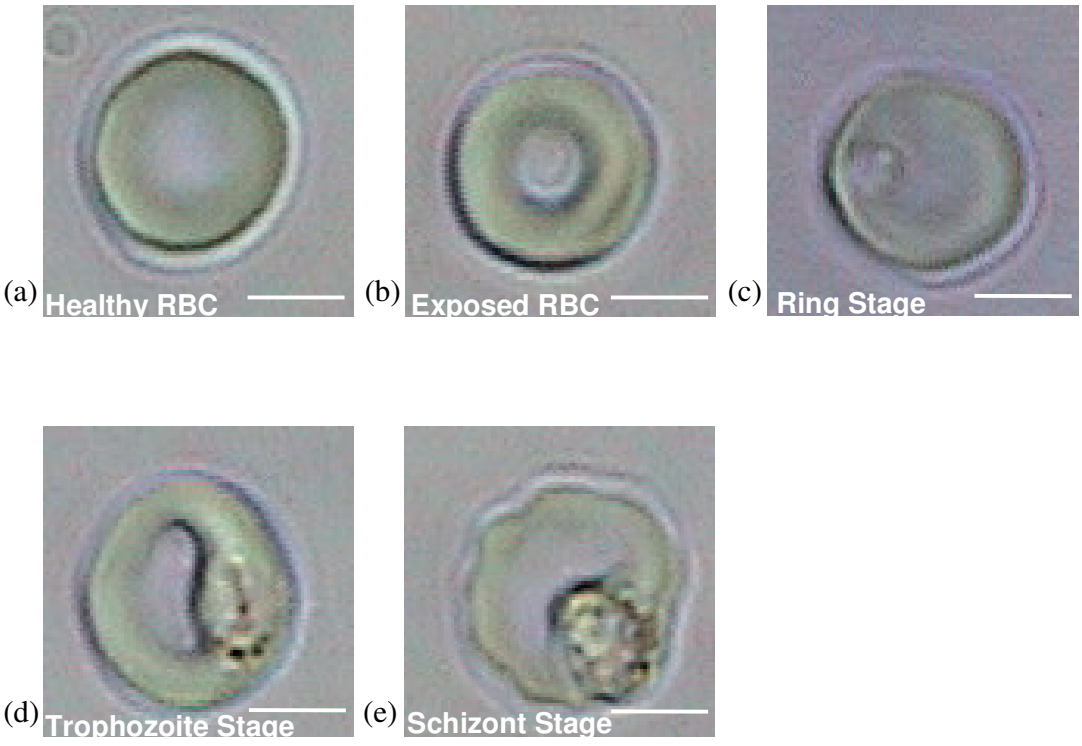

Figure 4.7 Optical micrographs of (a) healthy, (b) exposed to *Plasmodium yoelii* but uninfected, and *Plasmodium falciparum* parasitized human RBCs at (c) ring form, (d) trophozoite and (e) schizont stage. Scale bar: 4 µm

Table 4.2 The increase in diameter of mouse RBCs infected by *Plasmodium yoelii* in various developmental stages as well as those subjected to optical tweezers stretch tests in general (Test). Cell sizes are averaged from multiple measurements. Healthy: n=42; Ring Form n=18; Trophozoite n=20; Schizont n=38.

Cell Reference	Healthy	Ring Form	Trophozoite	Schizont	Test
Average Diameter (μm)	4.11	6.4	6.5	6.8	6.8
Enlargement (%)		**3.0**	**4.3**	**10.1**	**9.4**

Stretch data for mouse RBCs were obtained using the same procedures as those used for the human RBC tests (section 3.7). Because of noticeable variations in sizes of the cells being tested, the deformation was plotted as percentage changes, as shown in Figure 4.8. Variations in diameters of mouse red blood cells infected by different stages of *Plasmodium yoelii,* i.e., Py-R-RBC, Py-T-RBC and Py-S-RBC, stretched at different tensile forces demonstrated progressive increasing rigidity of the host cells. However, *Plasmodium yoelii* parasitization did not induce appreciable increase in stickiness of host cell membrane. Therefore there was a certain experimental difficulty in finding infected cells with properly attached silica beads for stretch tests. Due to this problem, the tests from ring stage infected RBCs only went up to 130.3 pN, as the attaching of silica beads to the ring form infected cells were not strong enough to hold them together at higher stretching forces. At the schizont stage, the host red cell could be stretched up to 124% of its axial diameter. In contrast, the healthy mouse RBC was able to achieve an average maximum elongation of 173%.

See supplementary material CD-ROM for the complete test data and selected stretch videos of *P. yoelii* infected mouse RBCs.

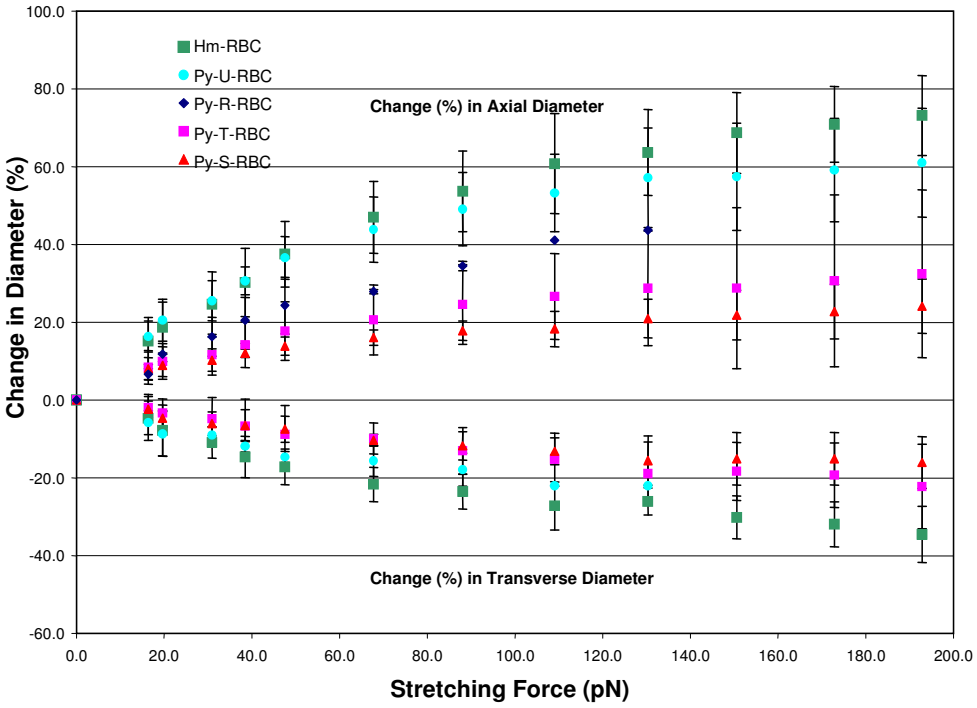

Figure 4.8 Plot of percentage change in axial and transverse diameter against stretching force of healthy, exposed, and *Plasmodium yoelii* infected RBCs stretched by optical tweezers. The vertical bars indicate scatter estimated by standard deviation of results from multiple repeat experiments.

The computational simulations based on these data employing different values of in-plane shear modulus were employed to match the experimental measurements, where modulus values of 10μN/m, 15μN/m, 40μN/m and 60μN/m were found to best match the experimental data for H-RBC, Py-U-RBC, Py-T-RBC and Py-S-RBC, respectively. The median values and range of shear modulus values of these simulations are incorporated with the human RBC data in the previous chapter in Figure 4.9.

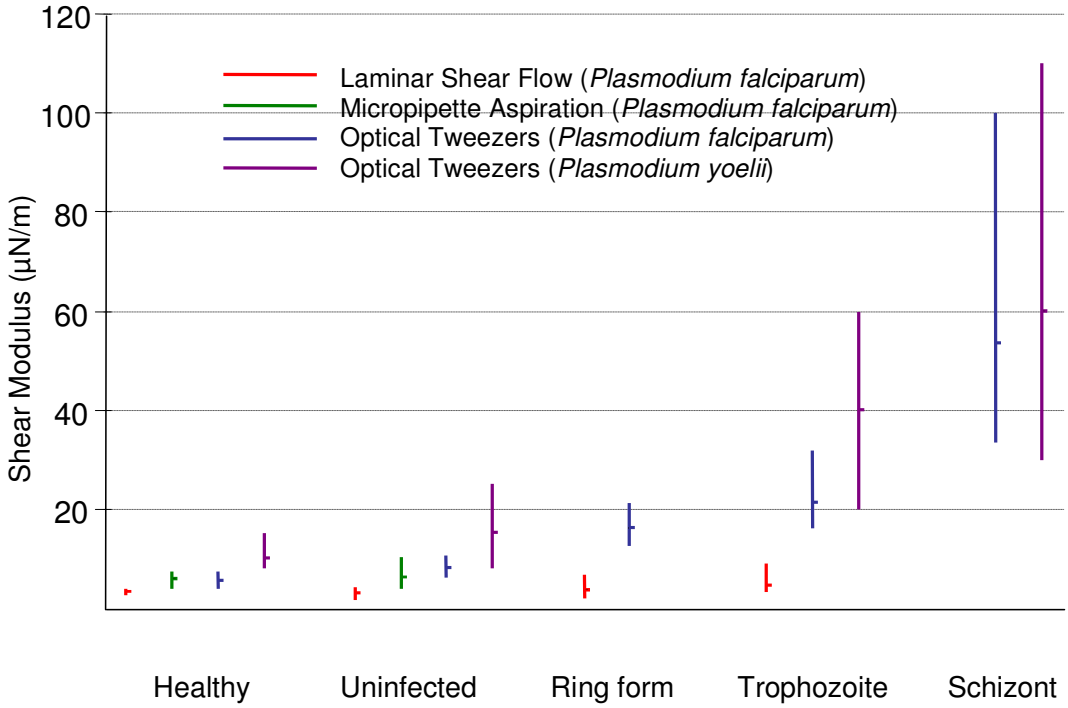

Figure 4.9 A combined chart of current available estimations of RBC stiffening response, comparing prior results on *Plasmodium falciparum* infected human RBCs based on micropipette aspiration [3] and laminar shear flow [7] methods, and present results on both *Plasmodium falciparum* infected human RBCs and *Plasmodium yoelii* infected mouse RBCS using optical tweezers method.

4.2.2 Discussion

The observations here on the *P. yoelii* infected mouse RBCs reveal parallel trends to that of human RBCs infected by *P. falciparum* which also demonstrated progressively reduced deformability with malaria parasites maturing within the host cells. While the schizonts of *P. falciparum* infected human RBCs were estimated to have a ten-fold increase of in-plane shear modulus when compared to uninfected blood cells, *P. yoelii* schizonts infected mouse RBCs only showed a six-fold increase. Whether this could

be due to the using of a non-virulent strain of *P. y. yoelii* or reasons essential to the mouse RBC itself requires further systematic investigation.

4.3 Fluorescent Visualization of Malaria RBCs Subjected to Optical Tweezers Stretching

DAPI binds differentially and highly specifically to nuclear DNA and has been widely used to visualized RBCs parasitized by malaria parasite. In Figure 4.10**,** (a) shows the overlap of optical and fluorescent image of a schizont stage *Plasmodium falciparum* infected human RBC, (b) is that of a mouse RBC parasitized by two schizont stage *Plasmodium yoelii* parasites.

(a) (b)

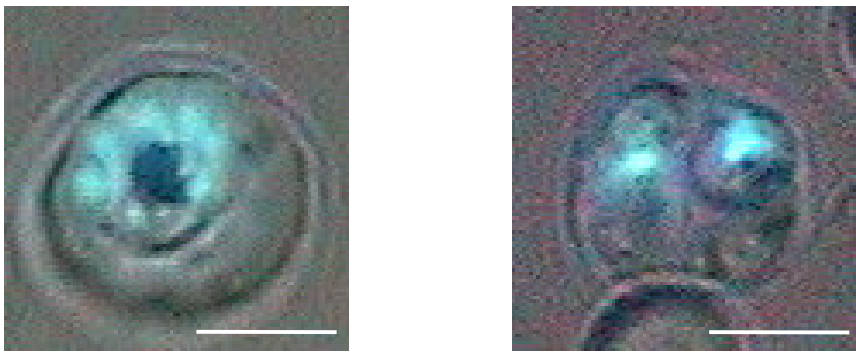

Figure 4.10 Micrographs of malaria infected RBCs with the nuclear DNA labeled by DAPI. The fluorescent signals were overlapped on top of the optical images. (a) A human RBC infected by a schizont stage *Plasmodium falciparum* parasite. The parasite has divided to produce several merozoites (bright blue dots). (b) A mouse RBC infected by two schizont stage *Plasmodium yoelii* parasites, as seen by two parasite vacuoles inside the cell. Scale bar: 4 μm

In order to incorporate *in situ* fluorescent visualization during stretch tests, DAPI stained malaria RBCs were prepared with similar procedures as that used for non-labeled cells. The bright field illumination was dimmed to optimize the fluorescent signal. Since DAPI stained preparations tend to fade rapidly, the fluorescence shutter was open only before the stretch tests started and photography should be immediately taken.

Figure 4.11 shows some snapshots taken from the digital video recording of a *Plasmodium falciparum* infected RBCs during stretch test. (The video of this test can be found in the supplementary material CD-ROM.) Fully occupied by the schizont stage parasite, which had multiplied into four merozoites indicated by the bright blue fluorescence from DAPI staining, the cell has nearly completely lost its deformability with no discernible elongation exhibited. While it revolved and swayed due to the stretching force, the three-dimensional structure of the cell and the parasite in the interior of it could be better visualized with aid of fluorescent labeling.

Based on the present observations of the stretch tests on the *Plasmodium falciparum* and *Plasmodium yoelii* infected RBCs labeled with DAPI, the infected cells appeared to have greater rigidity compared to the previous tests without DAPI labeling. It is unclear whether this is due to potential stiffening of the infected RBCs derived from DAPI staining.

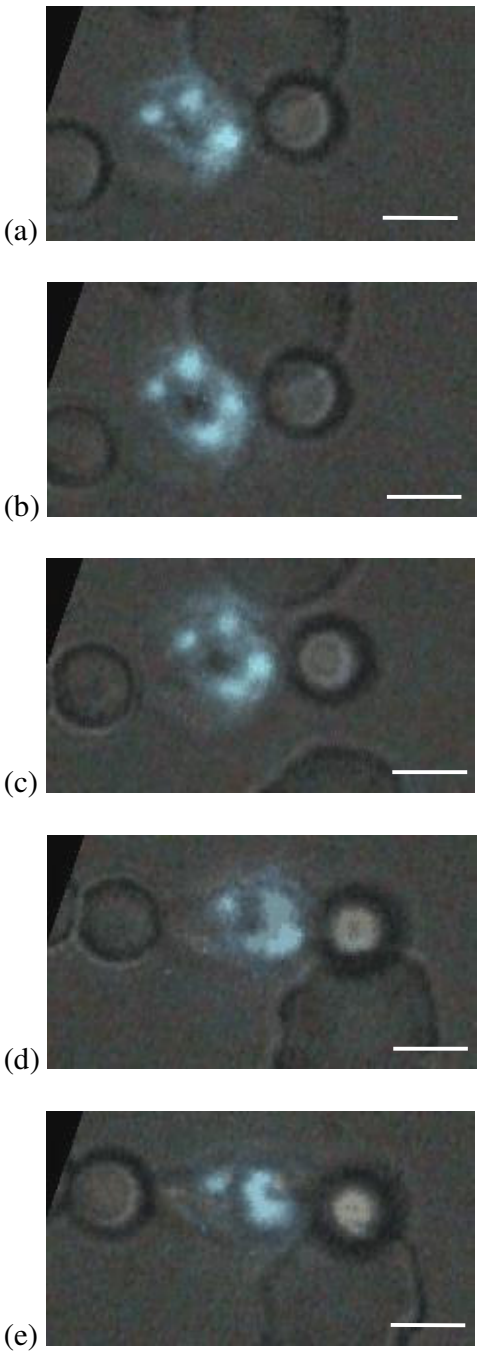

Figure 4.11 A human RBC infected with schizont stage *Plasmodium falciparum* stained with DAPI showing no discernible elongation even under a maximum stretching force of 193 pN. (a)-(e): successive images cropped out from stretching video. Scale bar: 4 μm

This approach of combining fluorescent visualization of the parasite with mechanical probing of the malaria parasitized RBCs is still at its primary stage. However, it does provide a promising first step in developing substantially expanded perception of the parasite-engineered internal structure of the host RBC. Information on the behavior of the parasite when the host cell is undergoing large deformation will provide us deeper understanding about the association between the parasite vacuole and the RBC cytoskeleton and membrane. This will further help us to understand the effect of the parasite on the stiffening of the RBC and will greatly benefit in providing more accurate mechanical modeling of the parasitized RBC.

Chapter 5: Conclusions and Recommendations

5.1 Conclusions

In this work, optical tweezers was used to study single living human and mouse red blood cells by inducing large tensile deformation. The first direct and continuous force–displacement curves for the progressive changes to the deformability of human RBCs parasitized to different developmental stages of *P. falciparum* malaria was obtained here. The *in-vitro* experimental measurements along with three-dimensional computational simulations provide a complete framework for the study of how the mechanics of deformation can be systematically and quantitatively probed as a function of the developmental stage of an infectious disease. Our observations of up to an order of magnitude increase in effective shear modulus of the parasitized RBCs suggest a greater influence on cell deformability due to malaria infestation.

In principle, the optical tweezers method provides a means to impose simple and well-controlled stress states, such as direct tensile stretching in small or large deformation, to biological cells. In this sense, it is complementary to, and conceptually simpler to interpret than, the widely used micropipette aspiration method [111, 128]. Possible complications arising from micropipette aspiration of malaria infected cells, such as stress concentration at the ends of the micropipette and adhesion of the infected cell to the inner walls of the micropipette, can potentially be circumvented in the optical tweezers method. Combining experiments with three-dimensional computational simulations of deformation, this method may offer new

framework with which alteration to mechanical characteristics of parasitized RBCs can be quantitatively probed. Therefore it further provides a possible means to investigate systematically of the malaria pathophysiology.

5.2 Recommendations

There are a few areas in which the current optical tweezers method could be improved. These are as follows:

1) A higher frame rate image capturing device can be employed to improve the image-processing capability. The maximum stretch force provided by the present optical tweezers setup with a 1.5 W 1064nm Nd:YAG laser is estimated to be about 193 pN. The next step would be to use a higher power laser (10 W) in order to generate more powerful tweezers and greater trapping force.
2) With the benefits of the fast developing optical tweezers technology, dual or multiple optical traps can be introduced and different stress states imposed on the cell can be systematically varied. Here multiple beads can be attached to the cell membrane, to obtain different stress states and the constitutive response of the cell membrane and cytoskeleton can be probed under different chemical and biological conditions. Optical tweezers stretching of cells in one and more directions is also amenable to three-dimensional computational simulations which can be used to guide and interpret experimental observations.

3) The present approach can easily be extended to examine the increased deformability of RBCs parasitized by *Plasmodium Vivax,* which interestingly in contrast to *P. falciparum*, have been shown to have greatly increased their deformability [7]. It can also serve as an *in vitro* benchmark for assessing specific contributions to mechanical deformability of the RBC from specific parasite proteins or different antimalarials.
4) While looking to the possibility of using more powerful laser tweezers to achieve larger cell deformation, one concern is the radiation damage to the cells from the laser. An optical stretcher technique has been developed and used to deform normal human RBCs and mouse fibroblasts [137], and recently to examine the changes in deformability during the progression of cancerous human breast epithelial cells [138]. By using two slightly divergent laser beams opposing each other, the light flux through the cell can be minimized, hence reduce the damage to the cell to a large extent. However, currently this technique can only induce an axial deformation of 14.1±0.3% in normal human RBCs. It would not be able to induce discernible deformation in malaria infected RBCs, especially later stages, which have shown significant increase in rigidity. If optical stretcher can be further developed to obtain larger surface force, it will certainly be another way we want to explore to study the malaria infected human RBCs.

References

1. Miller, L.H., *et al*., *The pathogenic basis of malaria.* Nature, 2002. **415**(6872): p. 673-9.
2. Cooke, B.M., N. Mohandas, and R.L. Coppel, *The malaria-infected red blood cell: structural and functional changes.* Adv Parasitol, 2001. **50**: p. 1-86.
3. Glenister, F.K., *et al*., *Contribution of parasite proteins to altered mechanical properties of malaria-infected red blood cells.* Blood, 2002. **99**(3): p. 1060-3.
4. Cranston, H.A., *et al*., *Plasmodium falciparum maturation abolishes physiologic red cell deformability.* Science, 1984. **223**(4634): p. 400-3.
5. Nash, G., *et al*., *Abnormalities in the mechanical properties of red blood cells caused by Plasmodium falciparum.* Blood, 1989. **74**(2): p. 855-861.
6. Paulitschke, M. and G.B. Nash, *Membrane rigidity of red blood cells parasitized by different strains of Plasmodium falciparum.* J Lab Clin Med, 1993. **122**(5): p. 581-9.
7. Suwanarusk, R., *et al*., *The deformability of red blood cells parasitized by Plasmodium falciparum and P. vivax.* J Infect Dis, 2004. **189**(2): p. 190-4.
8. Martini, F.H., *Fundamentals of Anatomy & Physiology, 6th ed.* 2004.
9. Nakao, M., *New insights into regulation of erythrocyte shape.* Current Opinion in Hematology, 2002. **9**(2): p. 127-132.
10. Mohandas, N. and J.A. Chasis, *Red blood cell deformability, membrane material properties and shape: regulation by transmembrane, skeletal and cytosolic proteins and lipids.* Semin Hematol, 1993. **30**(3): p. 171-92.
11. Singer SJ, N.G., *The fluid mosaic model of the structure of cell membranes.* Science, 1972. **175**(23): p. 720-31.
12. Bennett, V., *The Membrane Skeleton of Human Erythrocytes and its Implications for more Complex Cells.* Annual Review of Biochemistry, 1985. **54**(1): p. 273-304.
13. Bennett, V., *The spectrin-actin junction of erythrocyte membrane skeletons.* Biochim Biophys Acta., 1989. **988**(1): p. 107-21.
14. Bennett, V., *Spectrin-based membrane skeleton: a multipotential adaptor between plasma membrane and cytoplasm.* Physiol Rev., 1990. **70**(4): p. 1029-65.
15. Low, P.S., *Structure and Function of the Cytoplasmic Domain of Band 3: Center of Erythrocyte Membrane-Peripheral Protein Interactions.* Biochem. Biophys. Acta., 1986. **864**: p. 145-167.
16. Liu, S., L. Derick, and J. Palek, *Visualization of the hexagonal lattice in the erythrocyte membrane skeleton.* J. Cell Biol., 1987. **104**(3): p. 527-536.
17. Chasis, J. and N. Mohandas, *Erythrocyte membrane deformability and stability: two distinct membrane properties that are independently regulated by skeletal protein associations.* J. Cell Biol., 1986. **103**(2): p. 343-350.
18. Evans E, M.N., Leung A., *Static and dynamic rigidities of normal and sickle erythrocytes. Major influence of cell hemoglobin concentration.* J Clin Invest., 1984. **73**(2): p. 477-88.

19. Fortier N, S.L., Garver F, Kiefer C, McKenney J, Mohandas N., *The relationship between in vivo generated hemoglobin skeletal protein complex and increased red cell membrane rigidity.* Blood., 1988. **71**(5): p. 1427-31.
20. Schrier, S. and N. Mohandas, *Globin-chain specificity of oxidation-induced changes in red blood cell membrane properties.* Blood, 1992. **79**(6): p. 1586-1592.
21. Schrier SL, R.E., Mohandas N., *Cellular and membrane properties of alpha and beta thalassemic erythrocytes are different: implication for differences in clinical manifestations.* Blood., 1989. **74**(6): p. 2194-202.
22. Evans, E., R. Waugh, and L. Melnik, *Elastic area compressibility modulus of red cell membrane.* Biophys. J., 1976. **16**(6): p. 585-595.
23. Bannister, L. and G. Mitchell, *The ins, outs and roundabouts of malaria.* Trends Parasitol, 2003. **19**(5): p. 209-13.
24. Howard RJ, B.J., Kao V., *Antigenic variation of Plasmodium knowlesi malaria: identification of the variant antigen on infected erythrocytes.* Proc Natl Acad Sci U S A., 1983. **80**(13): p. 4129-33.
25. Leech, J., *et al*., *Identification of a strain-specific malarial antigen exposed on the surface of Plasmodium falciparum-infected erythrocytes.* J. Exp. Med., 1984. **159**(6): p. 1567-1575.
26. Waller, K.L., *et al*., *Mapping the Binding Domains Involved in the Interaction between the Plasmodium falciparum Knob-associated Histidine-rich Protein (KAHRP) and the Cytoadherence Ligand P. falciparum Erythrocyte Membrane Protein 1 (PfEMP1).* J. Biol. Chem., 1999. **274**(34): p. 23808-23813.
27. Oh, S.S., *et al*., *Plasmodium falciparum erythrocyte membrane protein 1 is anchored to the actin-spectrin junction and knob-associated histidine-rich protein in the erythrocyte skeleton*1.* Molecular and Biochemical Parasitology, 2000. **108**(2): p. 237-247.
28. Voigt, S., *et al*., *The cytoadherence ligand Plasmodium falciparum Erythrocyte Membrane Protein 1 (PfEMP1) binds to the P. falciparum Knob-associated Histidine-rich Protein (KAHRP) by electrostatic interactions.* Molecular and Biochemical Parasitology, 2000. **110**(2): p. 423-428.
29. Trager W, R.M., Bradbury PC., *The fine structure of Plasmodium falciparum and its host erythrocytes in natural malarial infections in man.* 1966. **35**(6): p. 883-5.
30. Stanley, H.A. and R.T. Reese, *Plasmodium falciparum Polypeptides Associated with the Infected Erythrocyte Plasma Membrane.* PNAS, 1986. **83**(16): p. 6093-6097.
31. Fernandez, V., *et al*., *Small, Clonally Variant Antigens Expressed on the surface of the Plasmodium falciparum-infected Erythrocyte Are Encoded by the rif Gene Family and Are the Target of Human Immune Responses.* J. Exp. Med., 1999. **190**(10): p. 1393-1404.
32. Helmby H , L.C., U Pettersson, and M Wahlgren, *Rosetting Plasmodium falciparum-infected erythrocytes express unique strain-specific antigens on their surface.* Infect Immun., 1993. **61**(1): p. 284-288.

33. Kilejian, A., *Characterization of a Protein Correlated with the Production of Knob-Like Protrusions on Membranes of Erythrocytes Infected with Plasmodium falciparum.* PNAS, 1979. **76**(9): p. 4650-4653.
34. Kilejian A, O.J., *Proteins and glycoproteins from human erythrocytes infected with Plasmodium falciparum.* Bull World Health Organ., 1979(57 Suppl 1): p. 101-7.
35. Crabb BS, C.B., Reeder JC, Waller RF, Caruana SR, Davern KM, Wickham ME, Brown GV, Coppel RL, Cowman AF., *Targeted gene disruption shows that knobs enable malaria-infected red cells to cytoadhere under physiological shear stress.* Cell., 1997. **89**(2): p. 287-96.
36. Kilejian A, R.M., Aikawa M, Aji T, Yang YF., *Selective association of a fragment of the knob protein with spectrin, actin and the red cell membrane.* Mol Biochem Parasitol., 1991. **44**(2): p. 175-81.
37. Magowan, C., *et al*., *Plasmodium falciparum histidine-rich protein 1 associates with the band 3 binding domain of ankyrin in the infected red cell membrane.* Biochimica et Biophysica Acta (BBA) - Molecular Basis of Disease, 2000. **1502**(3): p. 461-470.
38. Handunnetti SM, P.B., van Schravendijk MR, Aguiar JC, Taraschi TF, Gormley JA, Howard RJ., *The characterization of two monoclonal antibodies which react with high molecular weight antigens of asexual Plasmodium falciparum.* Mol Biochem Parasitol., 1992. **54**(2): p. 231-46.
39. Pasloske BL, B.D., Ma C, Taraschi TF, Gormley JA, Howard RJ., *PfEMP3 and HRP1: co-expressed genes localized to chromosome 2 of Plasmodium falciparum.* Gene., 1994. **144**(1): p. 131-6.
40. Waterkeyn, J.G., *et al*., *Targeted mutagenesis of Plasmodium falciparum erythrocyte membrane protein 3 (PfEMP3) disrupts cytoadherence of malaria-infected red blood cells.* EMBO J., 2000. **19**(12): p. 2813-2823.
41. Coppel RL, L.S., Murray L, Anders RF., *MESA is a Plasmodium falciparum phosphoprotein associated with the erythrocyte membrane skeleton.* Mol Biochem Parasitol., 1988. **31**(3): p. 223-31.
42. Howard RF, S.H., Reese RT., *Characterization of a high-molecular-weight phosphoprotein synthesized by the human malarial parasite Plasmodium falciparum.* Gene., 1988. **64**(1): p. 65-75.
43. Coppel RL, C.J., Bianco AE, Crewther PE, Stahl HD, Brown GV, Anders RF, Kemp DJ., *Variable antigen associated with the surface of erythrocytes infected with mature stages of Plasmodium falciparum.* Mol Biochem Parasitol., 1986. **20**(3): p. 265-77.
44. Howard, R., *et al*., *Transport of an Mr approximately 300,000 Plasmodium falciparum protein (Pf EMP 2) from the intraerythrocytic asexual parasite to the cytoplasmic face of the host cell membrane.* J. Cell Biol., 1987. **104**(5): p. 1269-1280.
45. Howard RJ, B.J., Rock EP, Neequaye J, Ofori-Adjei D, Maloy WL, Lyon JA, Saul A., *Two approximately 300 kilodalton Plasmodium falciparum proteins at the surface membrane of infected erythrocytes.* Mol Biochem Parasitol., 1988. **27**(2-3): p. 207-23.

46. Lustigman S, A.R., Brown GV, Coppel RL., *The mature-parasite-infected erythrocyte surface antigen (MESA) of Plasmodium falciparum associates with the erythrocyte membrane skeletal protein, band 4.1.* Mol Biochem Parasitol., 1990. **38**(2): p. 261-70.
47. Magowan, C., *et al*., *Role of the Plasmodium falciparum mature-parasite-infected erythrocyte surface antigen (MESA/PfEMP-2) in malarial infection of erythrocytes.* Blood, 1995. **86**(8): p. 3196-3204.
48. Waller, K.L., *et al*., *Mature parasite-infected erythrocyte surface antigen (MESA) of Plasmodium falciparum binds to the 30-kDa domain of protein 4.1 in malaria-infected red blood cells.* Blood, 2003. **102**(5): p. 1911-1914.
49. Chishti, A., *et al*., *Phosphorylation of protein 4.1 in Plasmodium falciparum-infected human red blood cells.* Blood, 1994. **83**(11): p. 3339-3345.
50. Petersen C, N.R., Magowan C, Wollish W, Jensen J, Leech J., *The mature erythrocyte surface antigen of Plasmodium falciparum is not required for knobs or cytoadherence.* Mol Biochem Parasitol., 1989. **36**(1): p. 61-5.
51. Coppel RL, C.A., Anders RF, Bianco AE, Saint RB, Lingelbach KR, Kemp DJ, Brown GV., *Immune sera recognize on erythrocytes Plasmodium falciparum antigen composed of repeated amino acid sequences.* Nature., 1984. **310**(5980): p. 789-92.
52. Perlmann, H., *et al*., *Antibodies in malarial sera to parasite antigens in the membrane of erythrocytes infected with early asexual stages of Plasmodium falciparum.* J. Exp. Med., 1984. **159**(6): p. 1686-1704.
53. Brown, G., *et al*., *Localization of the ring-infected erythrocyte surface antigen (RESA) of Plasmodium falciparum in merozoites and ring-infected erythrocytes.* J. Exp. Med., 1985. **162**(2): p. 774-779.
54. Aikawa M, T.M., Sjolander A, Berzins K, Perlmann P, Miller LH, *Pf155/RESA antigen is localized in dense granules of Plasmodium falciparum merozoites.* Exp Parasitol, 1991(7): p. 193.
55. Culvenor JG, D.K., Anders RF., *Plasmodium falciparum ring-infected erythrocyte surface antigen is released from merozoite dense granules after erythrocyte invasion.* Infect Immun., 1991. **59**(3): p. 1183-7.
56. Foley M, T.L., Sawyer WH, Anders RF., *The ring-infected erythrocyte surface antigen of Plasmodium falciparum associates with spectrin in the erythrocyte membrane.* Mol Biochem Parasitol., 1991. **46**(1): p. 137-47.
57. Ruangjirachuporn W, U.R., Carlsson J, Drenckhahn D, Perlmann P, Berzins K., *Plasmodium falciparum: analysis of the interaction of antigen Pf155/RESA with the erythrocyte membrane.* Exp Parasitol., 1991. **73**(1): p. 62-72.
58. Taylor DW, P.M., Chapman GB, Stearns ME, Rener J, Aikawa M, Uni S, Aley SB, Panton LJ, Howard RJ., *Localization of Plasmodium falciparum histidine-rich protein 1 in the erythrocyte skeleton under knobs.* Mol Biochem Parasitol., 1987. **25**(2): p. 165-74.
59. Taylor DW, P.M., Stearns ME., *Plasmodium falciparum: fine structural changes in the cytoskeletons of infected erythrocytes.* Exp Parasitol., 1987. **64**(2): p. 178-87.

60. Allred DR, G.J., Sherman IW., *Dynamic rearrangements of erythrocyte membrane internal architecture induced by infection with Plasmodium falciparum.* J Cell Sci., 1986(81): p. 1-16.
61. Parker, P.D., L. Tilley, and N. Klonis, *Plasmodium falciparum induces reorganization of host membrane proteins during intraerythrocytic growth.* Blood, 2004. **103**(6): p. 2404-2406.
62. Ling, E., Y. Danilov, and C. Cohen, *Modulation of red cell band 4.1 function by cAMP-dependent kinase and protein kinase C phosphorylation.* J. Biol. Chem., 1988. **263**(5): p. 2209-2216.
63. Dondorp, A.M., *et al*., *Abnormal Blood Flow and Red Blood Cell Deformability in Severe Malaria.* Parasitology Today, 2000. **16**(6): p. 228-232.
64. Hunt NH, S.R., *Oxidative stress and the redox status of malaria-infected erythrocytes.* Blood Cells., 1990(162-3): p. 499-526.
65. Lee MV, A.J., DeSouza JM, Lee RV., *Diminished red blood cell deformability in uncomplicated human malaria. A preliminary report.* J Med., 1982. **13**(5-6): p. 479-85.
66. JP Gardner, R.P., DJ Roberts, and CI Newbold, *Variant Antigens and Endothelial Receptor Adhesion in Plasmodium falciparum.* Proc Natl Acad Sci U S A., 1996. **93**(8): p. 3503-3508.
67. C Raventos-Suarez, D.K.K., F Macaluso, and R L Nagel, *Membrane knobs are required for the microcirculatory obstruction induced by Plasmodium falciparum-infected erythrocytes.* Proc Natl Acad Sci U S A., 1985. **82**(11): p. 3829-3833.
68. M Ho, B.S., S Looareesuwan, T M Davis, D Bunnag, and N J White, *Clinical correlates of in vitro Plasmodium falciparum cytoadherence.* Infect Immun., 1991. **56**(3): p. 873-878.
69. Hasler, T., *et al*., *In vitro rosetting, cytoadherence, and microagglutination properties of Plasmodium falciparum-infected erythrocytes from Gambian and Tanzanian patients.* Blood, 1990. **76**(9): p. 1845-1852.
70. Ockenhouse CF, H.M., Tandon NN, Van Seventer GA, Shaw S, White NJ, Jamieson GA, Chulay JD, Webster HK., *Molecular basis of sequestration in severe and uncomplicated Plasmodium falciparum malaria: differential adhesion of infected erythrocytes to CD36 and ICAM-1.* J Infect Dis., 1991. **164**(1): p. 163-9.
71. Ockenhouse, C., *et al*., *Human vascular endothelial cell adhesion receptors for Plasmodium falciparum-infected erythrocytes: roles for endothelial leukocyte adhesion molecule 1 and vascular cell adhesion molecule 1.* J. Exp. Med., 1992. **176**(4): p. 1183-1189.
72. Cooke BM, M.-J.S., Greenwood BM, Nash GB., *Mechanisms of cytoadhesion of flowing, parasitized red blood cells from Gambian children with falciparum malaria.* Am J Trop Med Hyg., 1995. **53**(1): p. 29-35.
73. Newbold C, W.P., Black G, Berendt A, Craig A, Snow B, Msobo M, Peshu N, Marsh K., *Receptor-specific adhesion and clinical disease in Plasmodium falciparum.* Am J Trop Med Hyg., 1997. **57**(4): p. 389-98.

74. Cooke, B.M., *et al*., *Assignment of functional roles to parasite proteins in malaria-infected red blood cells by competitive flow-based adhesion assay.* Br J Haematol, 2002. **117**(1): p. 203-211.
75. David PH, H.S., Leech JH, Gamage P, Mendis KN., *Rosetting: a new cytoadherence property of malaria-infected erythrocytes.* Am J Trop Med Hyg., 1988. **38**(2): p. 289-97.
76. Udomsangpetch, R., *et al*., *Plasmodium falciparum-infected erythrocytes form spontaneous erythrocyte rosettes.* J. Exp. Med., 1989. **169**(5): p. 1835-1840.
77. Rowe JA, M.J., Newbold CI, Miller LH., *P. falciparum rosetting mediated by a parasite-variant erythrocyte membrane protein and complement-receptor 1.* Nature., 1997. **388**(6639): p. 292-5.
78. Chen, Q., *et al*., *The Semiconserved Head Structure of Plasmodium falciparum Erythrocyte Membrane Protein 1 Mediates Binding to Multiple Independent Host Receptors.* J. Exp. Med., 2000. **192**(1): p. 1-10.
79. Antonio Barragan, P.G.K., Mats Wahlgren, Johan Carlson, *Blood Group A Antigen Is a Coreceptor in Plasmodium falciparum Rosetting.* Infect Immun., 2000. **68**(5): p. 2971-2975.
80. Urban BC, F.D., Pain A, Willcox N, Plebanski M, Austyn JM, Roberts DJ., *Plasmodium falciparum-infected erythrocytes modulate the maturation of dendritic cells.* Nature., 1999. **400**(6739): p. 73-7.
81. Vincke, I.H., and M. Lips., *Un nouveau plasmodium d'un rongeur sauvage du Congo: P. bergei.* Ann. Soc. Belg. Med. Trop., 1948(28): p. 94-104.
82. Walther H. Wernsdorfer, I.S.M., *Malaria: Principles and Practice of Malariology.* 1988.
83. Killick-Kendrick, R., *Parasitic protozoa of the blood of rodents: a revision of Plasmodium berghei.* Parasitology., 1974. **69**(2): p. 225-37.
84. A. Ashkin, J.M.D., J. E. Bjorkholm, Steven Chu, *Observation of a single-beam gradient force optical trap for dielectric particles.* Optics Letters, 1986. **11**(5): p. 288.
85. Ashkin, A., *Optical trapping and manipulation of neutral particles using lasers.* PNAS, 1997. **94**(10): p. 4853-4860.
86. Visscher K, B.G., Krol JJ., *Micromanipulation by "multiple" optical traps created by a single fast scanning trap integrated with the bilateral confocal scanning laser microscope.* Cytometry., 1993. **14**(2): p. 105-14.
87. Visscher, K.G., S.P. Block, S.M. and P.D.D. 1996, *Construction of multiple-beam optical traps with nanometer-resolution position sensing.* IEEE Journal of Selected Topics in Quantum Electronics, 1996. **2**(4): p. 1066-1076.
88. Svoboda, K. and S.M. Block, *Biological application of optical forces.* Annual Rev. Biophys. Biomed., 1994. **23**: p. 247-285.
89. Ashkin, A., *Forces of a single-beam gradient laser trap on a dielectric sphere in the ray optics regime.* Biophys. J., 1992. **61**: p. 569-582.
90. Kuo SC, S.M., *Force of single kinesin molecules measured with optical tweezers.* Science., 1993. **260**(5105): p. 232-4.
91. Wang, M., *et al*., *Stretching DNA with optical tweezers.* Biophys. J., 1997. **72**(3): p. 1335-1346.

92. Korda PT, T.M., Grier DG., *Kinetically locked-in colloidal transport in an array of optical tweezers.* Phys Rev Lett., 2002. **89**(12): p. 128301.
93. K. Ladavac, K.K.a.D.G.G., *Sorting by periodic potential energy landscapes: Optical fractionation,.* Physical Review E, 2004(70): p. 010901(R).
94. A. Terray, J.O., D.W.M. Marr, *Fabrication of Linear Colloidal Structures for Microfluidic Applications.* Applied Physics Letters, 2002(81): p. 1555.
95. Ashkin, A. and J.M. Dziedzic, *Internal Cell Manipulation Using Infrared Laser Traps.* PNAS, 1989. **86**(20): p. 7914-7918.
96. Block, S.M., Blair, D.F. and Berg, H.C., *Compliance of bacterial flagella measured with optical tweezers.* Nature, 1989(338): p. 514-518.
97. Ashkin, A., *et al*., *Force generation of organelle transport measured in vivo by an infrared laser trap.* Nature, 1990. **348**: p. 346-348.
98. Berg, H.C., *How spirochetes may swim.* J. Theor. Biol., 1976(56): p. 269-273.
99. Chu, S., *Laser Trapping of Neutral Particles.* Scientific American, 1992(266): p. 70-76.
100. SURESH, G.B.a.S., *Cell and molecular mechanics of biological materials.* Nature Materials, 2003(2): p. 715-725.
101. Mathur, A.B., *et al*., *Endothelial, cardiac muscle and skeletal muscle exhibit different viscous and elastic properties as determined by atomic force microscopy.* Journal of Biomechanics, 2001. **34**(12): p. 1545-1553.
102. Chen, J., *et al*., *Twisting integrin receptors increases endothelin-1 gene expression in endothelial cells.* Am J Physiol Cell Physiol, 2001. **280**(6): p. C1475-1484.
103. Evans E, Y.A., *Apparent viscosity and cortical tension of blood granulocytes determined by micropipette aspiration.* Biophys J., 1989. **56**(1): p. 151-60.
104. Usami S, C.H., Zhao Y, Chien S, Skalak R., *Design and construction of a linear shear stress flow chamber.* Ann Biomed Eng., 1993. **21**(1): p. 77-83.
105. Ellis EF, M.J., Willoughby KA, Liang S, Povlishock JT., *A new model for rapid stretch-induced injury of cells in culture: characterization of the model using astrocytes.* J Neurotrauma., 1995. **12**(3): p. 325-39.
106. Wang JH, G.-C.P., Yin FC., *Contractility affects stress fiber remodeling and reorientation of endothelial cells subjected to cyclic mechanical stretching.* Ann Biomed Eng., 2000. **28**(10): p. 1165-71.
107. Pfister BJ, W.T., Betenbaugh M, Bao G., *An in vitro uniaxial stretch model for axonal injury.* Ann Biomed Eng., 2003. **31**(5): p. 589-98.
108. Evans, E.A., *New membrane concept applied to the analysis of fluid shear- and micropipette-deformed red blood cells.* Biophys. J., 1973. **13**(9): p. 941-954.
109. Hochmuth, R.M., Mohandas, N., Blackshear, P.L., *Measurement of the elastic modulus for red cell membrane using a fluid mechanical technique.* Biophys. J., 1973. **13**(8): p. 747-762.
110. Hochmuth, R.M., Waugh, R.E., *Erythrocyte membrane elasticity and viscosity.* Ann. Rev. Physiol., 1987(49): p. 209-219.
111. Evans, E.A., Skalak, R., *Mechanics and Thermal Dynamics of Biomembranes.* CRC Press, Boca Raton, FL., 1980.

112. Ashkin, A., Dziedzic, J. M. and Yamane, T., *Optical Trapping and Manipulation of Single Cells Using Infrared-Laser Beams.* Nature, 1987. **330**: p. 769-771.
113. Svoboda, K., Schmidt, C. F., Branton, D. and Block, S. M., *Elastic Properties of Extracted Red-Blood-Cell Membrane Skeletons.* Faseb Journal, 1992(6): p. A523-A523.
114. Bronkhorst PJ, S.G., Grimbergen J, Nijhof EJ, Sixma JJ, Brakenhoff GJ., *A new method to study shape recovery of red blood cells using multiple optical trapping.* Biophys J., 1995. **69**(5): p. 1666-73.
115. Henon, S., *et al*., *A new determination of the shear modulus of the human erythrocyte membrane using optical tweezers.* Biophys J, 1999. **76**(2): p. 1145-51.
116. Simmons, R., *et al*., *Quantitative measurements of force and displacement using an optical trap.* Biophys. J., 1996. **70**(4): p. 1813-1822.
117. Discher, D.E., D.H. Boal, and S.K. Boey, *Simulations of the Erythrocyte Cytoskeleton at Large Deformation. II. Micropipette Aspiration.* Biophys. J., 1998. **75**(3): p. 1584-1597.
118. Boal, D., *Mechanics of the Cell.* Cambridge University Press 2002.
119. Sleep, J., *et al*., *Elasticity of the red cell membrane and its relation to hemolytic disorders: an optical tweezers study.* Biophys J, 1999. **77**(6): p. 3085-95.
120. Parker, K.H. and C.P. Winlove, *The Deformation of Spherical Vesicles with Permeable, Constant-Area Membranes: Application to the Red Blood Cell.* Biophys. J., 1999. **77**(6): p. 3096-3107.
121. Kellermayer, M.S.Z., *et al*., *Complete Unfolding of the Titin Molecule under External Force.* Journal of Structural Biology, 1998. **122**(1-2): p. 197-205.
122. Walliker D, Q.I., Wellems TE, McCutchan TF, Szarfman A, London WT, Corcoran LM, Burkot TR, Carter R., *Genetic analysis of the human malaria parasite Plasmodium falciparum.* Science., 1987. **236**(4809): p. 1661-6.
123. Trager, W. and J.B. Jensen, *Human malaria parasites in continuous culture.* Science, 1976. **193**(4254): p. 673-675.
124. Smith, T.G., *et al*., *Commitment to sexual differentiation in the human malaria parasite.* Parasitology (2000), 121:127-133 Cambridge University Press.
125. Dao, M., C.T. Lim, and S. Suresh, *Mechanics of the human red blood cell deformed by optical tweezers.* Journal of the Mechanics and Physics of Solids, 2003. **51**(11-12): p. 2259-2280.
126. Lim, C.T., *et al*., *Large deformation of living cells using laser traps.* Acta Materialia, 2004. **52**(7): p. 1837-1845.
127. Yeoh, O.H., *Characterization of Elastic Properties of Carbon-Black-Filled Rubber Vulcanizates.* Rubber Chem. Technol., 1990(63): p. 792-805.
128. Fung, Y., *Biomechanics: The mechanical properties of living tissues.* Springer-Verlag, New York, 1981.
129. Evans E, F.Y., *Improved measurements of the erythro- cyte geometry.* Microvasc. Res., 1972(4): p. 335-347.

130. Ashkin, A., *The study of cells by optical trapping and manipulation of living cells using infrared laser beams.* ASGSB Bull., 1991. **4**(2): p. 133-46.
131. Neuman, K.C., *et al*., *Characterization of Photodamage to Escherichia coli in Optical Traps.* Biophys. J., 1999. **77**(5): p. 2856-2863.
132. Schneckenburger, H., *et al*., *Cell viability in optical tweezers: high power red laser diode versus Nd:YAG laser.* Journal of Biomedical Optics, 2000. **5**(1): p. 40-44.
133. Svoboda, K., *et al*., *Conformation and elasticity of the isolated red blood cell membrane skeleton.* Biophys. J., 1992. **63**(3): p. 784-793.
134. Naumann, K.M., *et al*., *A Plasmodium falciparum exo-antigen alters erythrocyte membrane deformability.* FEBS Lett, 1991. **292**(1-2): p. 95-7.
135. Kaul, D., *et al*., *Microvascular hemodynamics and in vivo evidence for the role of intercellular adhesion molecule-1 in the sequestration of infected red blood cells in a mouse model of lethal malaria.* Am J Trop Med Hyg, 1998. **58**(2): p. 240-247.
136. Robinson, B.L., *Rodent Parasites Provide Laboratory Models.* MR4 Malaria Update, 2002(Oct).
137. Jochen Guck, R.A., Hamid Mahrnood, Tess J. Moon, C. Casey Cunningham, and Josef Kas, *The Optical Stretcher: A Novel Laser Tool to Micromanipulate Cells.* Biophys. J., 2001. **81**: p. 767-784.
138. Jochen Guck, S.S., Bryan Lincoln, Falk Wottawah, Susanne Ebert, Maren Romeyke, Dominik Lenz, Harold M. Erickson, Revathi Ananthakrishnan, Daniel Mitchell, Josef Kas, Sydney Ulvick, and Curt Bilby, *Optical Deformability as an Inherent Cell Marker for Testing Malignant Transformation and Metastatic Competence.* Biophys. J., 2005. **88**: p. 3689-3698.

LIST OF PUBLICATIONS

List of publications arising from this thesis work:

1. Mills, J. P., **Qie, L**., Dao, M., Lim, C.T. & Suresh, S. (2004) Experimental and computational study of nonlinear elastic and viscoelastic deformation of the red blood cell induced by optical tweezers. *Mechanics and Chemistry of Biosystems*. Vol. 1, no. 3, pp. 169-180

2. J. P. Mills, **L. Qie**, M. Dao, K. S. W. Tan, C. T. Lim, S. Suresh. Mechanical response of human red blood cells parasitized at different stages by Plasmodium falciparum malaria. Submitted for publication (2004)

3. J. P. Mills, **L. Qie**, M. Dao, K. S. W. Tan, C. T. Lim, S. Suresh. Continuous force-displacement relationships for the human red blood cell at different erythrocytic developmental stages of Plasmodium falciparum malaria parasite. *2004 Materials Research Society* **(***MRS) Fall Conference Proceedings.*

4. **L. Qie**, J. P. Mills, M. Dao, K. S. W. Tan, C. T. Lim, S. Suresh. Mechanical probing of human red blood cells (RBCs). *Oral presentation at the 2nd World Congress for Chinese Biomedical Engineers (WCCBME), September2004, Beijing, China*

APPENDIX:

Supplementary Materials: Data Sheets and Video Clips (CD-ROM)

The enclosed CD-ROM (affixed to the backcover of the thesis) contains the following supplementary materials:

In folder "Human"

HumanHealthyData.xls	Optical Tweezers stretching test data on healthy human RBCs
HumanMalariaData.xls	Optical Tweezers stretching test data on healthy as well as *P. falciparum* infected RBCs at different stages
HumanHealthy1.avi	Video clip on the optical tweezers stretching of a healthy human RBC at 193 pN
HumanHealthy2.avi	Video clip on the optical tweezers stretching of a healthy human RBC at 193 pN
HumanExposed.avi	Video clip on the optical tweezers stretching of an exposed human RBC at 193 pN
HumanRing.avi	Video clip on the optical tweezers stretching of a *P. falciparum* infected RBC at ring form stage at 193 pN
HuamnTrophozoite.avi	Video clip on the optical tweezers stretching of a *P. falciparum* infected RBC at trophozoite stage at 193 pN
HumanSchizont.avi	Video clip on the optical tweezers stretching of a *P. falciparum* infected RBC at schizont stage at 193 pN

In folder "Rodent"

MouseMalariaData.xls	Optical Tweezers stretching test data on healthy as well as *P. yoelii* infected RBCs at different stages

MouseHealthy.avi	Video clip on the optical tweezers stretching of a healthy Mouse RBC at 193 pN
MouseExposed.rm	Video clip on the optical tweezers stretching of an exposed Mouse RBC at 193 pN
MouseRing.avi	Video clip on the optical tweezers stretching of a *P. yoelii* infected RBC at ring form stage at 88 pN
HuamnTrophozoite.rm	Video clip on the optical tweezers stretching of a *P. yoelii* infected RBC at trophozoite stage at 193 pN
MouseSchizont.avi	Video clip on the optical tweezers stretching of a *P. yoelii* infected RBC at schizont stage at 193 pN

In folder "FluorescentLabeling"

HumanSchizontFluorescent.avi	Video clip on the optical tweezers stretching of a *P. falciparum* infected RBC stained with DAPI at schizont stage at 193 pN